Research of finger bone position and posture estimation method utilizing magnetic motion capture:

Development of skeletal finger model for estimating finger motion

(磁気式モーションキャプチャを用いた指骨の位置姿勢推定手法の研究：
手指動作推定のための手指スケルトンモデルの構築**)**

2019

Rong TANG

Akita University

Abstract

Motion capture is an important technology for surgical operation training, such as ergonomic assessment of hand motions in laparoscopic surgery. Researches relating to wrist angle and finger joint angles with glove-based motion capture device are available. However, hand motion and finger joint positions during laparoscopic surgery has not been discussed in previous researches because finger position measuring method for laparoscopic training has yet to exist within our knowledge. There are also some researches on dexterous movements using hand motion capture methods that applies methods such as optical motion capture. However, these researches are not related to laparoscopic training. To measure the hand motion of surgical operation when using scissor-like tools, such as laparoscopic instruments, the self-occlusion problem with optical motion capture cannot be avoided, as optical markers may be occluded by either the hands or surgical instruments. To address the occlusion problem, a magnetic motion capture device that is capable of finger motion measurement as magnetic field is able to pass through human body is useful solution. Another problem that needs to be addressed is the physical collision between the aforementioned instruments and magnetic receivers. When using scissor-like laparoscopic instruments, the handgrip may collide with magnetic receivers. In order to reduce these physical collisions, the number of receivers that placed on finger have to be reduced. As the result, skeletal finger model is necessary to estimate position finger segments that do not have receivers placed on them.

In this paper, we proposed a method to develop skeletal finger model for the estimation of finger motion when using scissor-like tools. We developed a calibration method for receiver posture, an estimation method for joint rotation center and rotation axis, and a joint center positions estimation method utilizing two receivers attached on fingertip and hand dorsum. In addition, we have measured and evaluated the motion of index finger which includes bone length (segmental length) and finger bone position by attaching receivers on the fingertip and hand dorsum during grasping. Furthermore, we compared the fingertip position generated by the proposed skeletal finger model to a finger model with rotation axes orthogonal to the finger bone.

For evaluating the skeletal finger model, we compared the fingertip positions generated by the proposed skeletal finger model to that of a finger model with rotation axes orthogonal to the finger bone. As the result, the mean (standard deviation) distance between the fingertips of all subjects and all target positions was

2.6 mm (0.9 mm). Compared to a finger model with rotation axes orthogonal to the finger bone, the mean error and standard deviation of the finger model generated by the proposed skeletal finger model was reduced by 45% and 47%, respectively. It is confirmed that the skeletal finger method generated by our method had better accuracy and reproduced a more realistic finger motion.

Further, we evaluated the mean segment lengths during a specified grasping motion were calculated by determining the position of joint centers. As the result, the standard deviations of all estimated segment lengths were under 0.2 mm. The positions of the joint centers obtained through our method with that obtained by attaching a full set of four receivers between the dorsal hand and index fingertip were compared. The Pearson correlation coefficients between the joint center positions estimated by our method and that of full set of receivers were calculated. The results showed a strong correlation between the joint center positions estimated by our method

Content

Chapter 1 Introduction

1-1 Background

Motion capture has developed and evolved along with the rapid progress in technology. Films and CG animation are well-known implementations of motion capture technology. From Star Wars in 1999 to Dawn of the Planet of the Apes in 2017, the motion of human beings has been tracked by motion capture devices and applied to CG models of humans or creatures in a fantasy world. In addition to use in the entertainment industry, motion capture has also been an active research topic since the 1980s [1]. For example, researchers adopted two tri-axial inertial sensors to measure the orientation of the arm, an upper limb motion estimation from inertial measurements, to aid in home-based rehabilitation of stroke patients [2]. By using motion capture technology with webcams, researchers were able to identify design principles that are important for upper limb stroke rehabilitation.

Nowadays, surgical operation training, such as for ergonomic assessment of hand motions in laparoscopic surgery, also utilize motion capture as an important technology. Research related to wrist angle and finger joint angles with glove-based motion capture (CyberGloveTM) are available [3]. In previous research, one 6 Degree-Of-Freedom (DOF) magnetic tracking sensor was mounted onto each needle holder, and the motion data of the sensors were recorded as the movement of laparoscopic instruments [4]. By analyzing the movements of laparoscopic instruments, it was possible to observe the differences between expert and novice surgeons.

Previous research, however, has not explored hand motion and finger joint positions during laparoscopic surgery because methods were unavailable for finger position measurement of laparoscopic training. While there has been some research on dexterous movements using hand motion capture methods that apply methods such as optical motion capture, such methods are still inadequate. Because of the self-occlusion problem when utilizing optical motion capture, past research has not tackled measurement of fine and complex movements, such as those involved in laparoscopic training.

In the measurement of the hand motion when using scissor-like tools during surgical operations, such as with laparoscopic instruments, either the hands or surgical instruments may occlude each other when capturing data with optical markers. To address the occlusion problem, it may be possible to utilize a magnetic

motion capture device that is capable of finger motion measurement as a magnetic field is able to pass through the human body. Another problem that needs to be addressed is the physical collision between the aforementioned instruments and magnetic receivers. When using scissor-like laparoscopic instruments, the handler may collide with magnetic receivers. In order to reduce these physical collisions, a skeletal finger model is necessary to estimate position finger segments that do not have receivers placed on them.

1-2 Purpose of this thesis

The purpose of this thesis is to develop a method to generate a skeletal finger model for the estimation of finger motion when using scissor-like tools, such as laparoscopic instruments. Details are as follows:

1. Development of calibration method for receiver posture.
2. Construction method of skeletal finger model: estimation method of joint rotation center, rotation axis and finger bone length (segmental length).
3. Estimation method of joint center positions utilizing two receivers attached on fingertip and hand dorsum.

1-3 Composition of this thesis

This thesis is composed of six chapters, each chapter introduces and discusses an aspect of developing a skeletal finger model for the estimation of finger motion when using scissor-like tools.

Chapter 1 introduced the importance and issues involved in hand motion capture, as well as the purpose of this thesis.

Chapter 2 describes the basics of motion measurement and analysis. The mechanism and characteristics of different types of motion capture are detailed, including inertial, optical, flex-sensor-based and magnetic. In addition, the construction of Hand-MoCap and the basics of analyzing motion capture by Hand-MoCap are described. Last, the skeletal finger model is also described, which is necessary for measuring dexterous motion.

Chapter 3 presents the construction of a measurement system for finger joint position and rotation axis, which includes the position measurement device, measurement system and target position for evaluating the end point of a finger. The experimental instructions, conditions and subjects are also introduced.

Chapter 4 proposes a construction and evaluation method for a skeletal finger model. In particular, this chapter introduces a construction method for a model that

captures both orthogonal axes and a user axis model. Furthermore, evaluations are done to consider variations of finger bone length, joint rotation axes and fingertip positions of both the orthogonal model and user axis model.

Chapter 5 describes the estimation and evaluation method for motion of finger segments that have no receivers. Results for both the orthogonal and user axis model are provided and discussed.

Chapter 6 concludes and offers suggestions for future works.

Chapter 2 Basics of motion measurement and analysis

This chapter introduces the basics for measuring finger motions, including the mechanisms utilized in current motion capture devices, a skeletal finger model and basics of motion analysis.

2-1 Mechanisms of various motion capture devices

Various motion capture devices with different mechanisms have been developed. There are generally five kinds of motion capture devices classified by mechanism and characteristics: inertial, optical, flex-sensor-based and magnetic. There is no perfect motion capture system, and each type has strong and weak points. The details are as follows:

2-1-1 Inertial motion capture

Inertial motion capture systems are usually constructed with inertial sensor modules that provide inertial data and a magnetic field. Some of these systems can even provide acceleration, roll/pitch and referenced yaw data. Current inertial sensors cannot obtain precise absolute position without an extra sensor and estimation. In order to reconstruct the motion of a performer, hierarchical models with body dimensions have to be constructed in advance. Furthermore, previous hierarchical models have typically been reconstructed through analysis of motion data that utilizes walking data [1].

Most inertial motion capture systems are usually wireless. This means that the quality of motion may drop if measurement conditions are poor due to wireless networks, such as conditions with multiple Wi-Fi spots. In recent years, two widely-used inertial motion capture systems are: the MVN System made by Xsens™ [2], and the Perception Neuron System made by Noitom™ [3]. Former one is magnetic immune and expensive, latter one has very high cost performance and low accuracy. Both systems are for full-body motion capture, and are not able to measure finger motion.

2-1-2 Optical motion capture

There are two common types of optical motion capture devices: marker-based type and marker-less type (camera-based motion capture). This section describes the advantages and disadvantage of both marker-based and camera-based motion capture.

2-1-2-1 Marker-based motion capture

Marker-based motion capture systems are constructed by utilizing cameras and optical markers. By recognizing the position of markers placed on the body, it is possible to reconstruct the body posture of the performer. Optical markers have to be placed on the body, either with flashing infrared LEDs or small infrared-reflecting dots. There are at least two cameras that surround a performer, and every camera allows for synchronization among the others in order to send video streams to a computer. The 3D position of markers is possible via triangulation with multiple 2D images from the cameras, and this is why at least two cameras are necessary. Therefore, a higher resolution in the cameras, usually means higher positioning accuracy. Another way to improve accuracy is to increase the number of cameras. By increasing the number of cameras, the risk of data loss can also be reduced, such as when markers were hidden in the blind spot of a particular camera. Apart from camera blind spots, marker-based systems have several other shortcomings:

1. Under conditions with strong light, such as outdoors, noise may be included in the data.
2. There must be enough space to place cameras.
3. Once markers were hidden from the camera, it is necessary to re-label the markers.

A typical optical motion capture system is made by VICON [4] or Optotrak [5]. For either hand motion capture or full-body motion capture, the VICON system needs calibration to provide determination of coordinates and the measurement range of each camera. Furthermore, similar to inertial motion capture, walking data is also necessary for full-body motion measurement [6].

2-1-2-2 Camera-based motion capture

Camera-based systems compute body motion parameters from extracted silhouettes, edges and other features. Camera-based motion capture devices are usually of a low cost, because a camera with a resolution of a million pixels can nowadays be easily obtained. However, camera-based systems can capture motion with only one camera, and there are several shortcomings:

1. Even with a depth sensor, accuracy drops when converted into 3D motion.
2. The self-occlusion (line of sight) problem may became severe because only one side of a performer is captured [7].

A typical camera-based motion capture system is Kinect produced by Microsoft™, which consists of a RGB camera, depth sensor and multi-array microphone [8].

Kinect is a motion capture device for the body, while the Leap Motion Controller is a popular device for hand motion capture [9]. There are three IR (Infrared) light emitters and two IR cameras [10] that receive the IR lights. By analyzing the IR images received by the camera, the Leap Motion Controller can detect palm and fingers movements on top of it. The Leap Motion Controller is usually used in hand gesture recognition, and finger joint position, direction, and velocity can be accessed by using its SDK. However, like other camera-based systems, the Leap Motion Controller also has the two shortcomings mentioned above.

2-1-3 Flex-sensor-based motion capture

Over the past decade, motion capture gloves have been developed, and most utilize flex sensors [11]. When grabbing or grasping, the flex sensors placed in the gloves will bend, which leads to attenuation of the light that passes through sensors. The difference in light is sent to a processor that determines joint angles. Because there are no extra devices like cameras, the measurement range is relatively larger than optical systems, and motion data is usually sent via wireless networks. There are, however, two shortcomings:

1. A motion capture glove uses the angle of a flex sensor as a joint angle, which may not be accurate enough under some conditions.
2. With parameters of the hand, it is possible to estimate the position of a finger joint, but errors in joint position may accumulate to the fingertip, and lead to significant positioning errors.

A typical flex-sensor-based motion capture system is Cyberglove, which has 18 or 22 flex sensors. Sensor resolution is within 1 degree, while repeatability is 3 degrees, and the data transfer technology is 802.11g Wi-Fi.

2-1-4 Magnetic motion capture

Magnetic motion capture systems are widely used for capturing movement due to their size, high sampling rate, resolution and no self-occlusion. Magnetic systems consist of sensors (receivers) and one transmitter. The coils in a receiver are placed in a sequence that creates three perpendicular fields. When magnetic fields pass through the coils in the receiver, the current is induced. The position and orientation (posture) of a receiver, which is relative to the transmitter can be calculated from the strength of the induced current. However, the shortcomings of a magnetic system are also related to the physical characteristics of magnetic fields.

1. Magnetic receivers are connected to a data processor with cables, compared to

marker-based motion capture devices that are wireless.

2. A magnetic field can easily be disturbed by ferromagnetic materials, and accuracy drops when the receiver is too close to the transmitters.

A typical magnetic motion capture device is the Liberty system made by Polhemus™, which is the system used in this research.

2-1-4-1 Liberty (Polhemus™)

Because we are measuring the motion of hands, which needs both the position and the orientation of finger segments, we have chosen the Liberty magnetic motion capture system. Our reasons are as follows:

1. Current inertial motion capture devices are focused on body measurement, and there is only one or even no sensor placed on each segment of a finger. As the result, there is no inertial motion capture device for estimating the position and posture of finger segments.
2. It is difficult to completely avoid the self-occlusion problem of an optical motion capture system when measuring hand motion.
3. A flex-sensor-based system cannot directly measure the position of finger segments.
4. The shortcomings of magnetic motion capture can be overcome with a proper measurement environment.

The Liberty system that we used measures motion data at a rate of 240 updates per second per receiver. The system comes standard with four sensor channels that can be upgraded to 8, 12 or 16. It has a latency of 3.5 ms, and a high resolution for both position and posture. Table 2.1 shows the relation between range and resolution [12].

Table 2.1 relation between range and resolution of Liberty.

Range[mm]	Resolution of position[mm]	Resolution of angle[°]
304.80	0.001422	0.000415
609.60	0.007239	0.001450
1219.00	0.130600	0.011768
2438.00	1.674000	0.172060

2-2 Basics of motion analysis with Hand-MoCap

Hand-MoCap is a magnetic motion capture system that we previously developed. In this section, the basics of motion analysis when using Hand-MoCap system are described. In particular, we review the data transformation between the measurement system and a CG animation system, method for producing a rotation matrix, method for calibrating posture data and a joint estimation method.

2-2-1 Construction of Hand-MoCap

In our previous research, we built Hand-MoCap, a motion capture system for the hand utilizing Liberty with 16 channels [13]. Further, we analyzed the dexterous finger movements of pianists and built an application for piano education [14]-[16]. Figure 2.1 shows the block diagram of Hand-MoCap. The system consists of a PC, a Liberty system and 16 receivers. All 16 receivers were placed on a hand, 3 on each finger and 1 on the dorsum of the hand. To fit the shape of the finger segments, the receivers placed on the hand were all processed into a teardrop shape. Toupee tape was used between the finger segments and receivers, and kinesiology tape was used to wrap the receivers onto the finger segments and nails. The measurement and analysis program were developed with Vizard 4.0 (WorldViz), a Python-based development platform. In addition, because the 3D modules were involved in the advanced version, Vizard was also used for CG animation in this thesis.

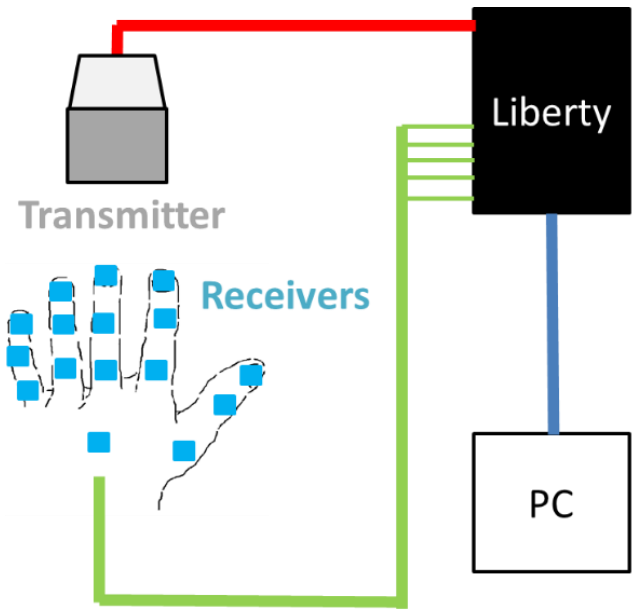

Figure 2.1 Block diagram of Hand-MoCap.

2-2-2 Coordinates of measurement system and CG animation system

The measurement system we used in this thesis is Hand-MoCap, which is based on the Liberty system made by Polhemus™. Therefore, the coordinates of the measurement system are based on the coordinates of the Liberty system transmitter. On the other hand, the animation system is based on the software Vizard, so it is necessary to transform the motion capture data from the measurement system coordinates to the animation system coordinates. Figure 2.2 shows the coordinates of the measurement system and CG animation system. The coordinates of the measurement system utilize a right-hand coordinate, while the coordinates of the animation system utilize a left-hand coordinate. Blue vectors represent the x axes, green vectors represent the y axes and red vectors represent z axes. The axes of the measurement system coordinates are noted with subscript m, while the animation system coordinates are noted with subscript a. The letter r represents the rotation angle of each axis, and the transformation functions are as follows.

$$\boldsymbol{x}_a = \boldsymbol{y}_m \ , \ \boldsymbol{y}_a = -\boldsymbol{z}_m \ , \ \boldsymbol{z}_a = \boldsymbol{x}_m \tag{2.1}$$

$$r_{xa} = -r_{ym} \ , \ r_{ya} = r_{zm} \ , \ r_{za} = -r_{xm} \tag{2.2}$$

In addition, the unit of length in the measurement system is inch, while it is meter in the animation system. Therefore, it is necessary to change the length from inch to meter in coordinate transformation. After all, the position of the transmitter remains as the origin of the animation system coordinates after transformation.

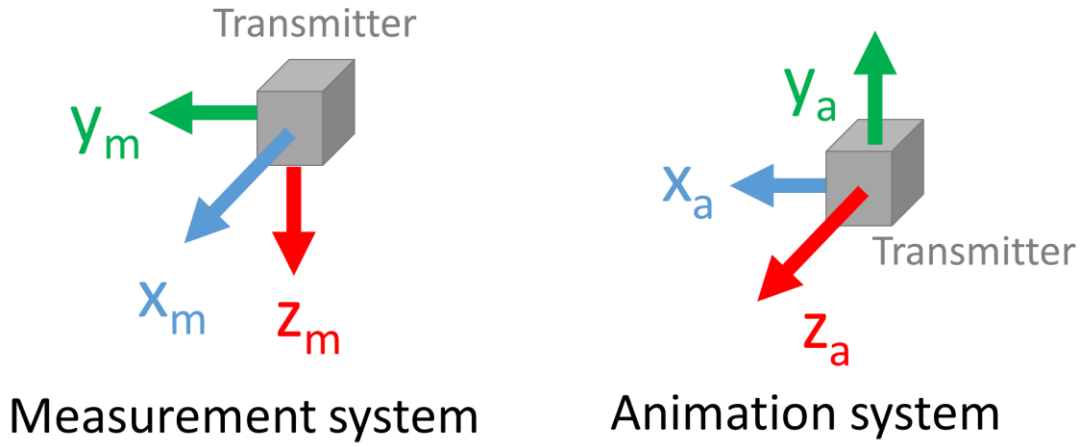

Figure 2.2 Coordinates of measurement and CG animation system.

2-2-3 Method for calibrating posture data of receivers

In this thesis, calibration means matching the posture data of receivers to the posture of finger bones. The motion data for calibration is captured under a static stretching posture, which is defined as the reference posture. Figure 2.3 shows the reference posture for calibrating the index finger. All fingers and the dorsum of the hand are placed on the table while the fingers are calibrated as pointing to the transmitter.

2-2-3-1 Basic version of calibration

For the Hand-MoCap system, there are two levels of calibration: the basic version and advanced version. The basic version of calibration is done under the assumption that all axes of a local coordinate of each receiver can be transformed from the coordinate of the transmitter. Figure 2.4 shows the basic version of calibration. Vectors with subscript *w* represent the base vector of the world coordinate, while vectors with subscript *l* represent the base vector of each receiver. In this version, all receivers have the same local coordinate. From the function

$$\boldsymbol{x}_l = \boldsymbol{z}_w \ , \ \boldsymbol{y}_l = -\boldsymbol{x}_w \ , \ \boldsymbol{z}_l = -\boldsymbol{y}_w \tag{2.3}$$

the base of the receivers can be calculated. From the base vector $\boldsymbol{x}_l , \boldsymbol{y}_l , \boldsymbol{z}_l$, the rotation matrix of the local coordinate at the reference posture $\mathbf{R}_r$ can be calculated. If $\mathbf{R}_{cal}$ is the rotation matrix calculated from the posture data of the receiver at the reference posture, and $\mathbf{R}_m^i$ represents the rotation matrix calculated from the *i* frame of motion data, the calibration function is

$$\mathbf{R}_a^i = \mathbf{R}_m^i \mathbf{R}_{cal}^{-1} \mathbf{R}_r \tag{2.4}$$

where $\mathbf{R}_a^i$ is the rotation matrix of the posture data after calibration. The advantage of basic calibration is the low computational cost. This calibration method was used in our past research that did not require high accuracy. As shown in Figure 2.4 (a), from the view of the x-z plane, the local coordinate seems to match with the finger segments. However, from Figure 2.4 (b), we can find that, because of the difference in thickness of each finger segments, the x axes and z axes should be different in different local coordinates of the segments.

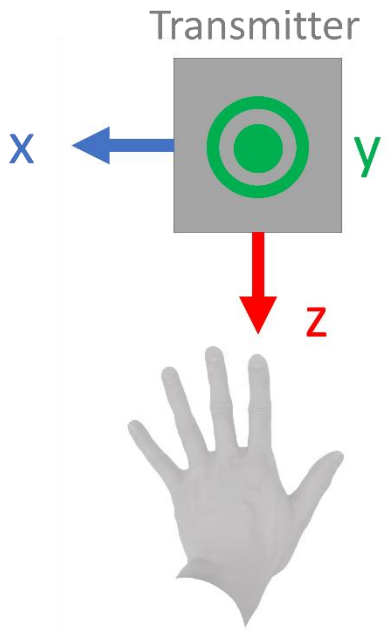

Figure 2.3 Reference posture.

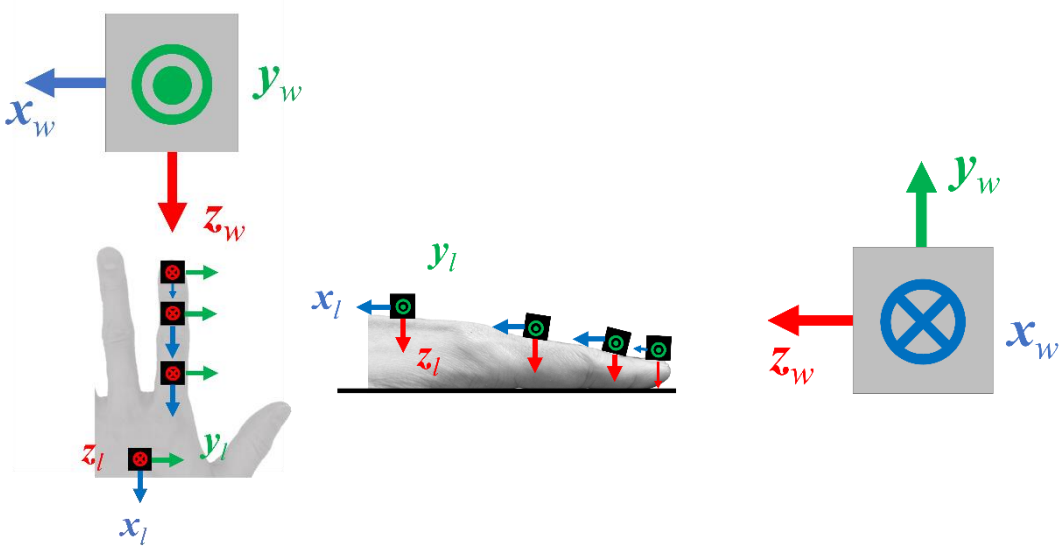

(a) x-z plane. (b) z-y plane.

Figure 2.4 Basic version of calibration.

2-2-3-2 Advanced version of calibration

Considering the thickness of the hand and the error at the reference posture, we proposed an advanced version of the calibration method. In this calibration method, we calculate the base vectors of the local coordinate from the joint rotation center (the specific calculation is described in Chapter 4). The local coordinate of the receiver placed on the dorsum of hand in the advanced version is the same as the basic version, while the calibration method for the other receivers are different. Figure 2.5 shows the advanced version of the calibration. The red points represent the position of each joint rotation center. From the joint rotation center of the MP, PIP and DIP joint, the vector represents the proximal phalanx $\boldsymbol{v}_p$ and the vector represents the middle phalanx $\boldsymbol{v}_m$, which can be calculated. In this advanced version of calibration, we define the vector that represents distal phalanx $\boldsymbol{v}_d = \boldsymbol{v}_m$, and the local x of each coordinate as follows:

$$\boldsymbol{x}_p = \frac{\boldsymbol{v}_p}{\|\boldsymbol{v}_p\|} \ , \ \boldsymbol{x}_m = \frac{\boldsymbol{v}_m}{\|\boldsymbol{v}_m\|} \ , \ \boldsymbol{x}_d = \frac{\boldsymbol{v}_d}{\|\boldsymbol{v}_d\|} \tag{2.5}$$

Furthermore, we defined the y axes as

$$\boldsymbol{y}_l = \boldsymbol{x}_l \times \boldsymbol{y}_w \tag{2.6}$$

where $\boldsymbol{x}_l$ (including $\boldsymbol{x}_p$, $\boldsymbol{x}_m$ and $\boldsymbol{x}_d$ in e.q. (2.5)) and $\boldsymbol{y}_l$ represents the local coordinate of each finger segment and $\boldsymbol{y}_w$ represents the coordinate of the transmitter. Then, the vector represents the z axes of a local coordinate

$$\boldsymbol{z}_l = \boldsymbol{x}_l \times \boldsymbol{y}_l \tag{2.7}$$

By applying equation (2.5), (2.6) and (2,7), it is possible to calculate the base vectors of the receivers placed on a finger. From these base vectors, the rotation matrix of each receiver can be expressed as $\mathbf{R}_p$, $\mathbf{R}_m$ and $\mathbf{R}_d$. The posture data of the receivers can then be calibrated by replacing the $\mathbf{R}_{cal}$ in equation (2.4) with $\mathbf{R}_p$, $\mathbf{R}_m$ and $\mathbf{R}_d$.

The advanced version of calibration can be processed after estimation of the joint rotation center, which leads to a high cost in performance. However, with the specific calculation for each segment, the posture after calibration is more accurate. Furthermore, by defining $\boldsymbol{v}_d = \boldsymbol{v}_m$, the x axes of the finger segments are acquired from calculation. Therefore, it is no longer necessary to point at the transmitter at the reference posture and this reduces potential human error when pointing at the transmitter.

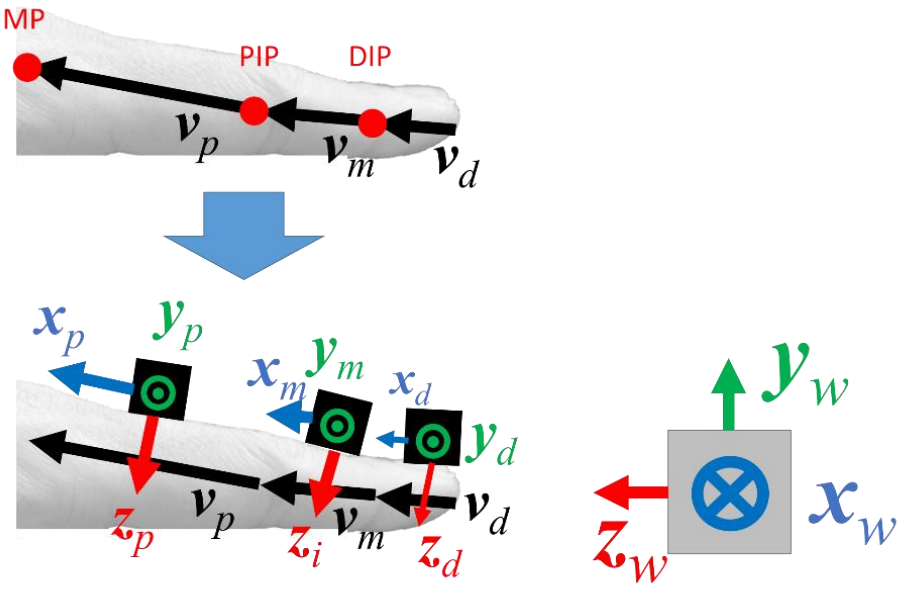

Figure 2.5 Advance version of calibration.

2-3-3 AJPE method

The AJPE method is an abbreviation from the title Automatic Joint Parameter Estimation from Magnetic Motion Capture Data presented by O'Brien [17]. The original paper presented a method estimate of joint parameters of the human body (without fingers), which also has been used to construct a hierarchical structure. The joint center estimation method that is used in full-body measurement, is defined as the AJPE method and is used in this thesis. Figure 2.6 the estimation method of joint rotation center in AJPE. Blue boxes represent the receivers placed on body segments. The center positions of the receivers are represented by $\boldsymbol{p}_1$ and $\boldsymbol{p}_2$, while $\boldsymbol{p}_{c1}$ and $\boldsymbol{p}_{c2}$ represent the rotation center estimated from each receiver. Let the $\mathbf{R}_1$ and $\mathbf{R}_2$ be the rotation matrix of each receiver, $\boldsymbol{p}_{c1}$ and $\boldsymbol{p}_{c2}$ can be described as:

$$\boldsymbol{p}_{c1} = \boldsymbol{v}_1\mathbf{R}_1 + \boldsymbol{p}_1 \ , \ \boldsymbol{p}_{c2} = \boldsymbol{v}_2\mathbf{R}_2 + \boldsymbol{p}_2 \tag{2.8}$$

where $\boldsymbol{v}_1$ and $\boldsymbol{v}_2$ are the vectors from the center of the receiver to the joint rotation center. Ideally $\boldsymbol{p}_{c1} = \boldsymbol{p}_{c2}$, so equation 2.8 can be rewritten as:

$$\boldsymbol{v}_1\mathbf{R}_1 + \boldsymbol{p}_1 = \boldsymbol{v}_2\mathbf{R}_2 + \boldsymbol{p}_2 \tag{2.9}$$

By solving $\boldsymbol{v}_1$ and $\boldsymbol{v}_2$ with singular value decomposition, the joint rotation center can be calculated from the data of both receiver 1 and receiver 2 with low error. The equation (2.8) and (2.9) is only a part of AJPE, which defined as the Modified AJPE method in this thesis.

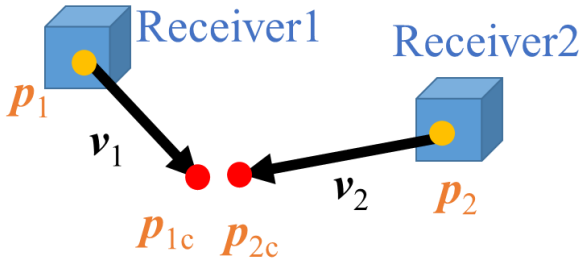

Figure 2.6 Estimation method of joint rotation center in AJPE.

2-3 Skeletal finger model

This section introduces the definition and details for a skeletal finger model, including generic definitions and the definition utilized in this thesis.

2-3-1 Definition of a skeletal model

In this thesis, a skeletal model does not mean that the model looks like a skeleton, and instead represents the mathematic model functions of movement by a human skeleton, which is represented by vectors. In motion capture analysis, the skeletal model may also be referred to as the kinematic model.

Most human joints are of a rolling contact joint type, and bones are in contact with each other as they roll around each other. The center of rotation and axis of rotation will shift with changes in joint angles. However, by calculating the approximation of center of rotation and axis of rotation to generate a skeletal model, it is possible to generate the motion of the body in CG animation and for control of a robot hand.

In CG animation of a human, there are two main components to the models, a skeletal model and a mesh model. A skeletal model includes the length of body segments, parameters for a joint such as center or axis. Meanwhile, the mesh model describes the 'meat' of the human body [18]. By moving the skeletal model manually or using motion capture data, movements of the body can be generated. To make a natural-moving CG animation for a human, the mesh model has to be attached to a skeletal model.

In comparison, only a skeletal model is used to control a robot hand. In 2000, Ude and other developers proposed an approach for constructing a skeletal model for the generation of humanoid robot motions based on observed human motion [19] [20]. However, only the few patterns of postures can be successfully controlled.

2-3-2 Definition of a skeletal finger model

The skeletal model discussed above generically means a full-body model, and all fingers are grouped together as hand. In other words, full-body motion captures are not considering detailed finger movements. In this thesis, we are focusing on finger motion analysis, and as such we propose a skeletal finger model.

The human hand is comprised of a total 27 bones, including 8 carpals, 5 metacarpals and 14 phalanxes [21]. In this thesis, we only consider the metacarpals and phalanges. Figure 2.7 shows the anatomical details and local coordinate system of a skeletal finger model. The yellow line represents the finger bones of the index finger. The origin of a local coordinate is defined at the distal end of each bone. The x axes

of each coordinate are towards the proximal end of bone, while the y axes are towards the direction of abduction, and the z axes are vectors from the dorsum side to the palm side of the hand.

2-4 Summary

This chapter describes the basics of motion measurement and analysis. The mechanism and characteristics of different types of motion capture are detailed, including inertial, optical, flex-sensor-based and magnetic. In addition, the construction of Hand-MoCap and the basics of analyzing motion capture by Hand-MoCap are described. Last, the skeletal finger model is also described, which is necessary for measuring dexterous motion. Next chapter describes the construction of measurement system for finger motion.

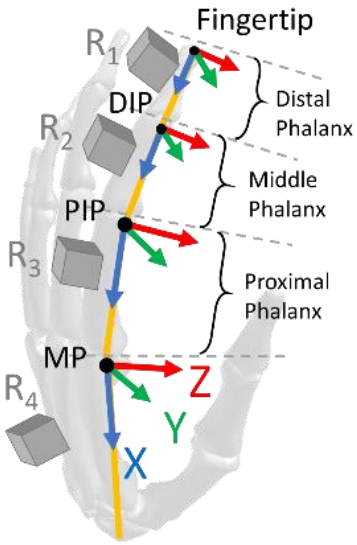

Figure 2.7 Anatomical detail and local coordinate system of a skeletal finger model.

<References>

[1] D. Roetenberg, H. Luinge, P.r Slycke, “Xsens MVN: Full 6DOF Human Motion Tracking Using Miniature Inertial Sensors,” XSENS TECHNOLOGIES white paper, (2013).

[2] MVN motion capture system, https://www.xsens.com/ (2018.12.01).

[3] Perception Neuron, https://neuronmocap.com/ (2018.12.01).

[4] VICON, https://www.vicon.com/ (2018.12.01).

[5] Optotrak, https://www.ndigital.com/ (2018.12.01).

[6] A.G. Kirk, J.F. O’Brien, D.A. Forsyth, “Skeletal parameter estimation from optical motion capture data,” IEEE Computer Society Conference on Computer Vision and Pattern Recognition, pp.782-788, (2005).

[7] L.Y. Chang, N.S. Pollard, “Constrained Least-Squares Optimization for Robust Estimation of Center of Rotation,” Journal of Biomechanics, Vol.40, No.6, pp.1392-1400, (2007).

[8] Kinect, https://developer.microsoft.com/en-us/windows/kinect (2018.12.01).

[9] Leap Motion, https://www.leapmotion.com/ (2018.12.01).

[10] F. Weichert, D. Bachmann, et al, “Analysis of the Accuracy and Robustness of the Leap Motion Controller,” Sensors, Vol. 13, No.5, pp.6380-6393, (2013).

[11] D.J. Sturman, D. Zeltzer, “A survey of glove-based input,” IEEE Computer graphics and Applications, (1994).

[12] Liberty, https://polhemus.com/_assets/img/LIBERTY_Brochure_1.pdf (2018.12.06).

[13] K. Mitobe, J. Kodama, T. Miura, M. Suzuki, N. Yoshimura, “Development of the learning assist system for dexterous finger movements,” ACM SIGGRAPH ASIA 2010 Posters, No.30, (2010).

[14] Md. M. Rahman, K. Mitobe, M. Suzuki, N. Yoshimura, “Analysis of Finger Movements of a Pianist Using Magnetic Motion Capture System with Six Dimensional Position Sensors,” Virtual Real. Soc. Jp., Vol.15, No.2, pp.243-250, (2010).

[15] Md. M. Rahman, K. Mitobe, M. Suzuki, N. Yoshimura, “Application of Hand Motion Capture System for Piano Education,” Virtual Real. Soc. Jp., Vol.16, Issue.1, pp.83-92, (2011).

[16] Md. M. Rahman, K. Mitobe, M. Suzuki, C. Takano, N. Yoshimura, “Analysis of dexterous finger movement for piano education using motion capture system,” Inter. J. Sci. Technol., Vol.2, Issue.2, pp.22-31, (2011).

[17] J.F. O'Brien, R.E. Bodenheimer, G.J. Brostow, J.K. Hodgins, "Automatic joint parameter estimation from magnetic motion capture data," Graphics Interface Conference, pp.53-60, (2000).

[18] Y. Endo, S. Kanai, T. Kishinami, N. Miyata, M. Kouchi, M. Mochimaru, "Optimization-Based Grasp Posture Generation Method of Digital Hand for Virtual Ergonomic Assessment," SAE International Journal of Passenger Cars - Electronic and Electrical Systems, Vol.1, No.1, pp.590-598, (2009).

[19] A. Ude, C. Man, M. Riley, CG. Atkeson, "Automatic Generation of Kinematic Models for the Conversion of Human Motion Capture Data into Humanoid Robot Motion," In Proc. First IEEE-RAS int. Conf. Humanoid Robots, IEEE Press, (2000).

[20] J. Butterfaß, M. Grebenstein, H. Liu, G. Hirzinger, "DLR-Hand II: Next generation of a dexterous robot hand," In Proc. IEEE Int. Conf. Robotics and Automation, pp.109-114, (2001).

[21] L.D. Richard, A. Wayne Vogl, "Gray's Anatomy for Students" Churchill Livingstone, an imprint of Elsevier Inc, pp.752-753, (2010).

Chapter 3 Construction of finger motion measurement system and experiment

This chapter introduces the details of measurement system and information about experiment.

3-1 Construction of measurement system for finger joint position and rotation axes

This section introduces a positioning device the stylus and the measurement system for finger joint position and rotation axes. The stylus is used not only in the measurement of target position, but also used in measuring the position of middle point on the skin of finger joint. Both measurement and evaluation system are described in this section.

3-1-1 Position measuring device: stylus

The stylus is a device for measuring position, with one receiver fixed on the thicker end of a pencil that is like wood. In order to get the calibration data of the stylus, the sharper end point is fixed on the test bench, and movement of the other end point is of a sphere surface. Figure 3.1 shows the motion for the stylus and the end point calculation method. Figure 3.1 (a) shows the motion for calibration. The curved blue vector represents the trajectory of receiver during calibration, and the black point represents the reference point fitted from the spherical motion data. The calibration data is a spherical motion data measured before experiment. Operator have to hold the thicker end of the stylus, which the receiver is placed on, to draw circles while remaining the shaper end at the same position. The start of calibration motion is from the posture that stylus is perpendicular with the table. Thereafter, incline the stylus at about 45 degree and start to draw circles to make trajectory like a sphere. From the stylus calibration data, the sharper point of the other end could be calculated by sphere fitting [1]. Figure 3.1 (b) shows the calculation method for the end point of the stylus. Once the vector ($\boldsymbol{v}_{\text{stylus}}$) between the receiver and the sharper end point is determined in the local coordinate of a receiver, the position of the sharper end point could be calculated from motion data. In this thesis, the mean and standard deviation distance from the position measured by the stylus and reference point are 0.5 mm and 0.3 mm, respectively. Figure 3.2 shows a sample of the distance between reference point and the end position measured by stylus. The distance at

the start is nearly 0 mm, became greater during circle-drawing, and back to 0 mm at the end of calibration where stylus is at the same posture of start.

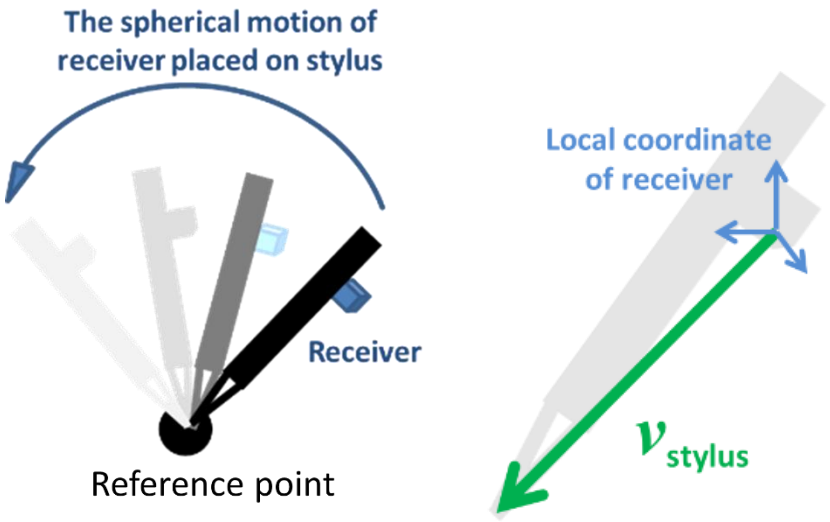

(a) Motion for calibrating stylus. (b) Calculation method of end point.

Figure 3.1 Motion for calibration and end point estimation method for stylus.

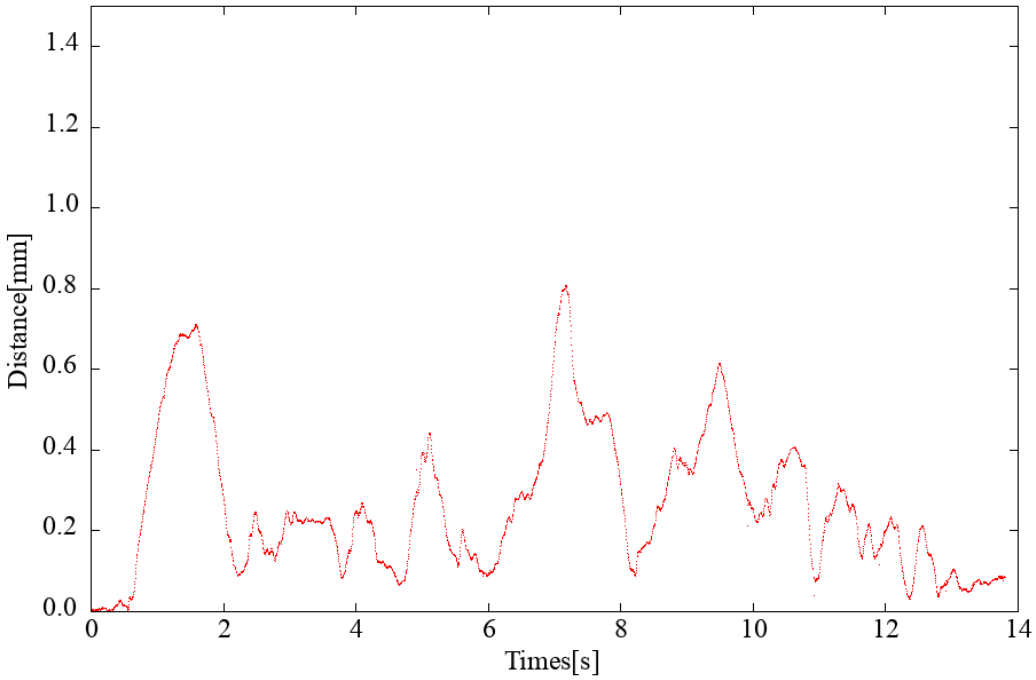

Figure 3.2 A sample of the distance between reference point and the end position measured by stylus.

3-1-2 Measurement system

Figure 3.3 shows the block diagram of the measurement system. Our Measurement system consists of a PC (Dell Latitude E6520 Note book), Polhemus™ Liberty system, one transmitter (TX4), five receivers and the Target which is made of chemical wood.. Four receivers are placed on each finger segment and the dorsum of a hand, and one receiver is placed on a stylus. The receivers measure position (x, y, z) and posture (yaw, pitch, roll) relative to the transmitter. Four receivers were placed on a hand, and one on a stylus. The stylus is a device for measuring position and details including calibration methods, which have been introduced in 3-1-1. The stylus is used to measure the target position on the edge of Target, which is used in the evaluation. The cylinder is at 38.0 mm diameter and 260.0 mm height, which is placed on the table when practicing grasping motion. To fit the shape of the finger segments, the receivers placed on the hand were all processed into a teardrop shape. Toupee tape was used between the finger segments and receivers, and kinesiology tape was used to wrap the receivers onto the finger segments and nails.

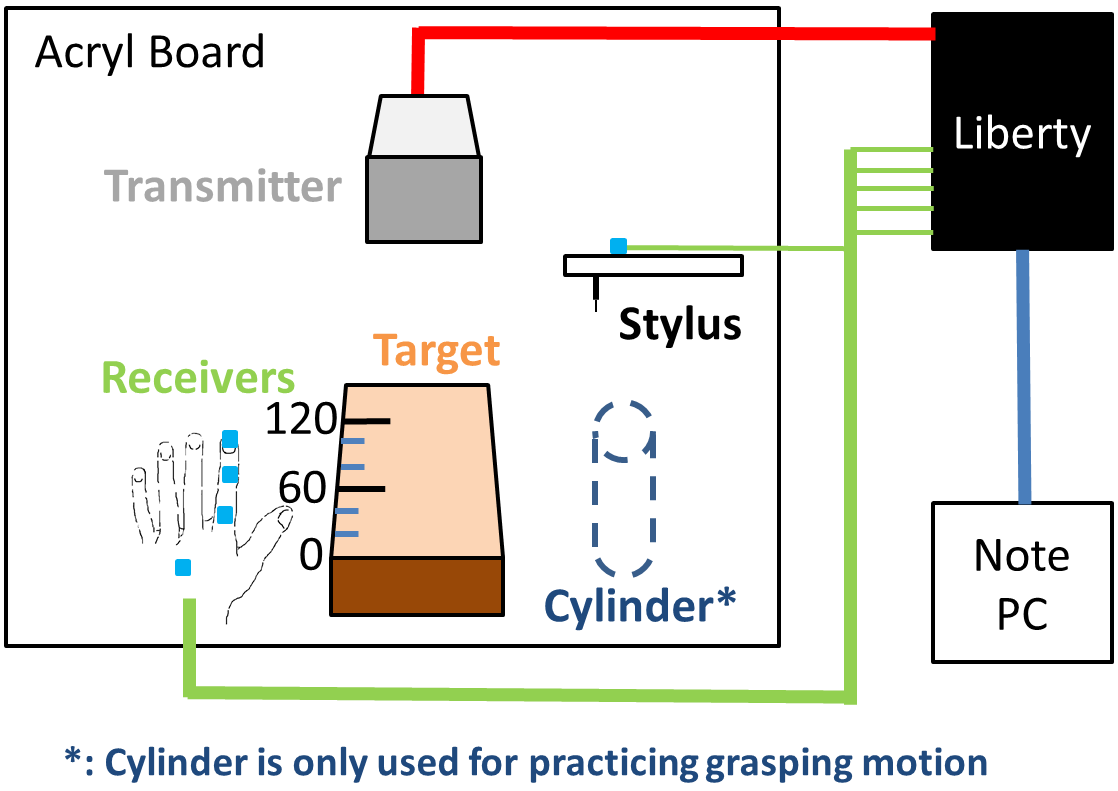

Figure 3.3 Block diagram of the experiment system.

3-1-3 Target for evaluating fingertip (end point)

To evaluate the robustness of the estimation method for axis of rotation and center of rotation, previous research has discussed the standard deviation of the distribution, which means the calculation itself is robust [2], [3]. However, it remains to be seen whether the axis of rotation and center of rotation function correctly in a skeletal finger model. In this paper, in order to evaluate skeletal finger model, we evaluated the accuracy of the fingertip position, which includes the accuracy of axis of rotation, center of rotation and segmental length. With segmental length and center of rotation calculated at the reference position, the fingertip position of the skeletal model during movements were calculated by rotating the distal phalanx about the axis of rotation of the DIP joint, and the position of the DIP joint was calculated from the coordinates of the middle phalanx and joint angle of DIP.

Figure 3.4 shows the positional relationship between the finger and the target used in the evaluation. Nakazawa and other developers proved that the trajectories and angle of writ are difference when people grasping a cylindrical object at different positions [4]. Therefore, as it is shown in Figure 3.3, the target positions which are made on the Target is placed in the front of subjects. Figure 3.4 (a) shows the coordinates of the Target and the arrangement of target positions. The size of the Target is L 140 mm ×W 100 mm ×L 50 mm. The origin of the Target is on the 0 mm target, and target positions were arranged on the Z axis. The target positions are 0.7 mm notches with a 20 mm gap between each other, from 0 mm to 120 mm. Figure 3.4 (b) shows changes in finger angle when reaching the different target positions. Subjects were directed to put the middle point of the thumb fingerprint onto the edge (0 mm position), while the other fingers grip naturally in a way that the subjects felt were comfortable. The change of distance between the index and thumb also reflects a change of joint angle, and the fingertips under a specific distance between the thumb and index were evaluated. The position of targets were estimated by the stylus, and the mean value of five measurements were used as the reference value.

3-2 Conditions and instructions in experiment

This section describes the finger motion for skeletal model generation, and the instructions and conditions in experiment.

3-2-1 Finger motion for skeletal model construction

The main process of the skeletal model generation is the estimation of rotation axis. For estimating the rotation axis of finger joints, the rotation around every joint have

to be involved in. The motion of grasping a circular cylinder has been used in previous research for building a skeletal hand model of the human hand [5]. Figure 3.5 shows the grasping motion. The motion is a sequence of grasping motion. However, if grasping the cylinder when capturing the motion, the palm of finger deforms when reaching the cylinder. And the deformation of finger palm may influent the orientation of receivers, which leads to noise in motion data. Therefore, as it is shown in Figure 3.3, the cylinder is only used for practicing, subjects are doing grasping motion without cylinder.

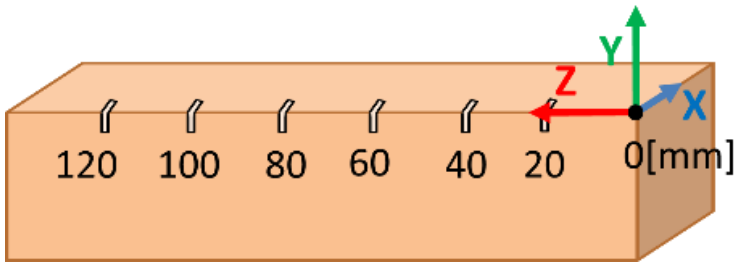

(a) Coordinate of target.

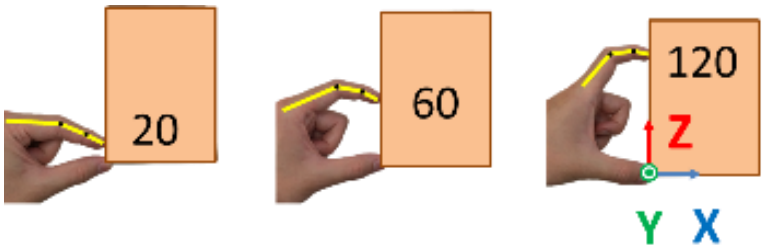

(b) Changes in finger angle.

Figure 3.4 Positional relation between finger and the target in evaluation of axis of rotation.

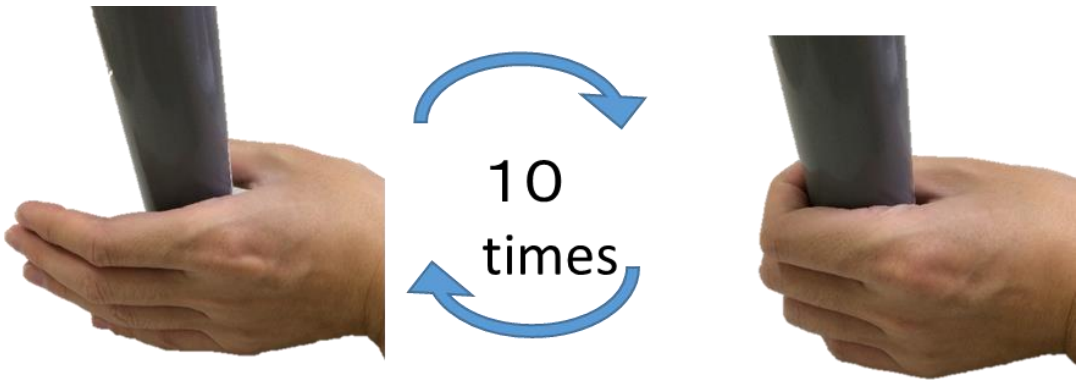

Figure 3.5 Grasping motion (repeat of flexion and extension).

3-2-2 Instructions

The experiment is divided into two parts, one is the motion for construction of skeletal finger model, another is for the evaluation of endpoint.

3-2-2-1 Motion measurement for the construction of skeletal finger model

The instructions, when measuring the motion for the construction of skeletal finger model, are as follows:

1. Subjects were ordered to relax and extend their wrist naturally.
2. When grasping the cylinder, except thumb finger, all fingers have to be closed to each other while grasping.
3. Subjects were ordered to practice the grasping motion at a tempo of two seconds.
4. Subjects have to do the grasping motion ten times without cylinder when in the measurement. The motion is start at an extending posture, a set of grasping and extending is count as one time.

All instructions and conditions are confirmed with recorded video data after measurement.

3-2-2-2 Motion measurement for evaluation of endpoint

The instructions, when measuring the motion for evaluation of endpoint, are as follows:

1. Subjects were ordered to bend middle, ring and pinky fingers while capturing motion.
2. Subjects were ordered to match their palm of thumb finger to the 0 mm on the Target.
3. Subjects were ordered to match their fingertips of index to the Target, from 20 mm to 120 mm, which is shown in Figure 3.4 (b).
4. Subjects were ordered to keep the same posture when match their fingertips to a position on the Target, until experimenter confirmed that their fingertips were well match to the each position on the Target.

All instructions are confirmed by experimenter during experiments.

3-3 Subjects

There are two groups of people participated in our experiments. The first group is with five men about twenty three years old on average. They participated in the evaluation and construction method of skeletal finger model, which is discussed in Chapter 4. The experiments in this thesis are applied ethical review in advance, and

permitted by research ethic committee.

3-4 Summary

This chapter describes the measurement system used in this thesis, which is comprised of a high resolution motion capture system (Hand-MoCap), a positioning device the stylus, a cylinder and the Target with target positions on. Furthermore, the experimental instructions and conditions are introduced. The next chapters are going to introduce the results of experiments.

<References>

[1] V. Pratt, “Direct least-squares fitting of algebraic surfaces,” Computer Graphics Vol.21, pp.145-152, (1987).

[2] S.S.H.U. Gamage, J. Lasenby, “New least squares solutions for estimating the average centre of rotation and the axis of rotation,” Journal of Biomechanics, Vol.35, Issue 1, pp.87-93, (2002).

[3] P. Cerveri, N. Lopomo., A. Pedotti., G. Ferrigno, “Derivation of centers and axes of rotation for wrist and fingers in a hand kinematic model: robust methods and reliability results,” Ann. Biomed. Eng., Vol.33, Issue.3, pp.401-411, (2005).

[4] N. Nakazawa, Y. Yoshihara, A. Fujinoki, T. Matsui, K. Yamada, I. Itoh, “Experimental study on precision grasp with respect to a cylindrical object - Path planning and contacted postion of digits,” Journal of Japan Ergonomics Society, Vol.42, No.2, pp.98-104, (2006).

[5] B. Buchholz, T. Armstrong, “A kinematic model of the human hand to evaluate its prehensile capabilities,” Journal of Biomechanics, Vol.25, No.2, pp.149-162, (1992).

Chapter 4 Construction method and evaluation of the skeletal finger model

This chapter describes the generation and evaluation method of the skeletal finger models. The generation method includes, the joint rotation axes, joint center, and construction method of the skeletal finger model. Thereafter, the differences between the typical skeletal finger model and our proposed skeletal finger model are introduced. Last, the evaluations of skeletal finger, are also introduced, including the results of the rotation axes, finger bone length and fingertip positions.

4-1 Construction method of skeletal finger model

This section describes the generation method of the skeletal finger model. The skeletal finger generated with the method introduced in this thesis is based on the motion data of individuals, which means the parameters of the skeletal finger models are different from each other. Figure 4.1 shows the overview of the construction method of skeletal finger model. The boxes represent each part of this method, black vectors represent specific methods and red vectors represent the data that output from each boxes. There are three main steps for construction of a finger model: motion measurement, estimation of joint rotation center and axes, and construction of a skeletal finger model.

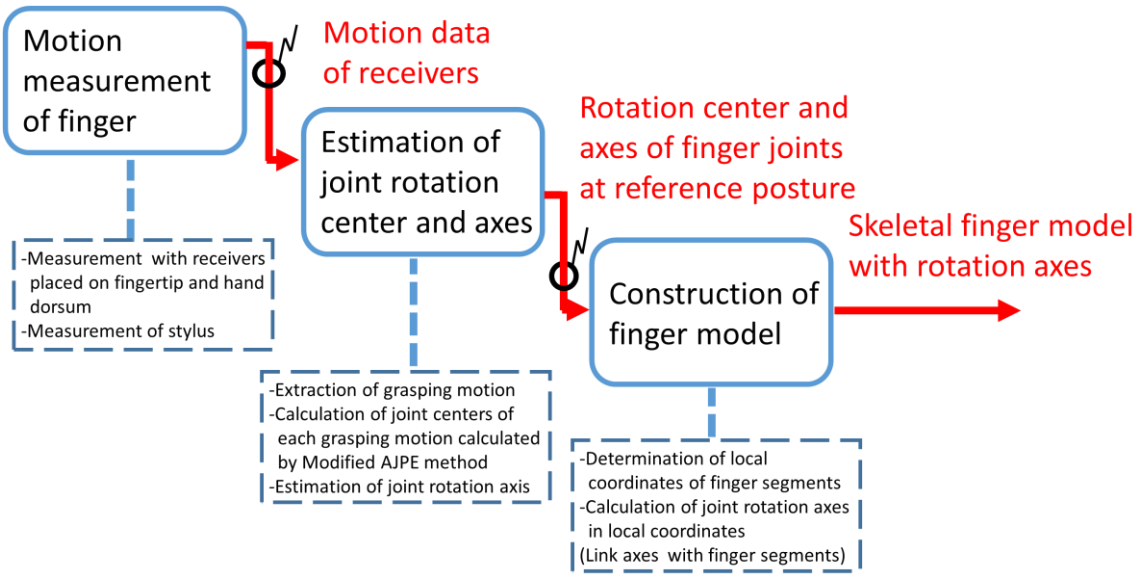

Figure 4.1 Overview of the construction method of skeletal finger model.

4-1-1 Measurement of finger motion

There are two groups of data. One is the hand motion data, which is introduced in Chapter 3, and the other includes the measurements with the stylus at the reference posture. The reference posture is a stretched posture, which is used for the calibration of the posture data of receivers. In order to evaluate the fingertip when reaching the target position, we also measured the middle point of the distal edge of the finger nail. Because the palm side of the finger deforms when touching a target, we defined the middle point of the distal edge of the finger nail as the fingertip (end point) position of the skeletal finger model. In order to evaluate the fingertip when reaching the target position, we also measured the middle point of the distal edge of the fingernail. Figure 4.2 shows a sample of the sagittal plane of the index finger. The red plane represents the sagittal plane.

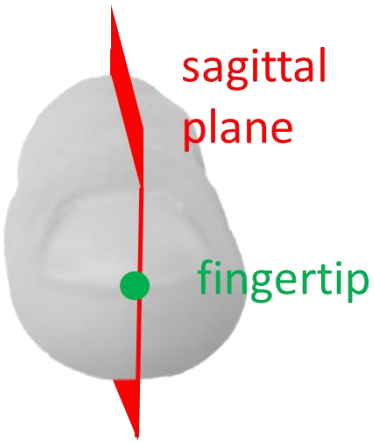

Figure 4.2 Sagittal plane of index finger.

4-1-2 Estimation method of joint rotation axes

The estimation method consists of several steps: extraction of the grasping motion, estimation of joint rotation center, and estimation of the joint rotation axis. Figure 4.3 shows one sample of the data extracted from a series of grasping motions. When capturing a series of positions within the grasping motion, there is always a short period of time in which the hand is just holding the cylinder or stretching, during which the motion data is almost static. Accuracy drops significantly if this kind of data is included in the estimation processing for the center of rotation and axis of rotation. Furthermore, a grasping motion is the combined movement of the Distal Interphalangeal (DIP) Joint, Proximal Interphalangeal (PIP) Joint, and Metacarpophalangeal (MP) Joint, and the dynamic and static periods for each joint are slightly different. Therefore, it is impossible to mark the start and end times manually, and it is necessary to have a method for extracting the grasping motion of each finger joint. Thus, we calculated the angle of the joint and angular velocity and the period $\Delta \boldsymbol{t_i}$ $(i \in \{1,\ 2, \ldots, 9, 10]\})$ of the grasping motion, which can be calculated from the angular velocity.

With the grasping motion data extracted from the raw data, it is possible to calculate the rotation axis. Figure 4.4 shows the estimation method for the rotation axis from a grasping motion. The equation for the axis of rotation is as follows:

$$\boldsymbol{J}(\boldsymbol{a}) = \sum_{i=1}^{10} |\boldsymbol{a} \times (\boldsymbol{c}_i - \boldsymbol{e})|^2 \tag{4.1}$$

Where $\boldsymbol{a}$ is AOR, $\boldsymbol{c}_i$ is the COR of the i th grasping motion, and $\boldsymbol{e}$ is one point on the AOR [1]. In this thesis, $\boldsymbol{e}$ is the average point of $\boldsymbol{c}_i$, and $\boldsymbol{c}_i$ is calculated from the data at $\Delta \boldsymbol{t_i}$. The calculation method of $\boldsymbol{c}_i$ is the AJPE method developed by J. F. O'Brien [2], which we discussed in Chapter 2.

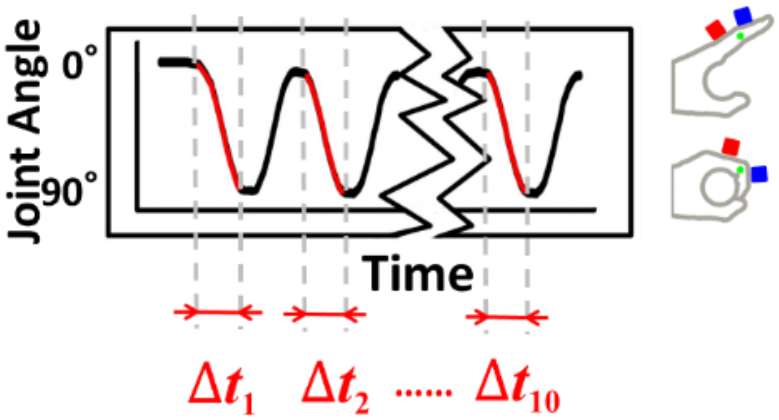

Figure 4.3 One sample of data extracted from a grasping motion series.

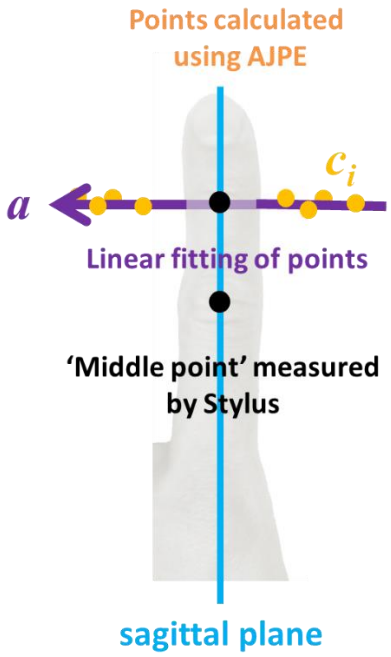

Figure 4.4 Estimation method for rotation axis from a grasping motion series.

4-1-3 Estimation method of the joint rotation center

The estimation of the joint rotation center is based on the results of the rotation axes. Figure 4.5 shows the joint center estimation method at the reference posture. In this thesis, postures are represented by the Euler angle (yaw pitch roll). The reference posture is the posture for defining the Euler angle of the finger segments. Using the stylus, the position of the midpoint on the skin can be measured. The normal vector of the sagittal plane is the same as the x axis of the coordinates of the transmitter. Therefore, with the midpoint on the DIP and PIP joint, it was possible to determine the sagittal plane of a finger. We defined the intersection of the joint axis and sagittal plane as the joint center for the DIP and PIP joint. To reduce calculation costs, we also used the same method as applied to the DIP and PIP joint on the metatarsophalangeal joint (MP joint). Although the MP joint is not biometrically a single-axis joint, there is a rotation axis in the grasping motion.

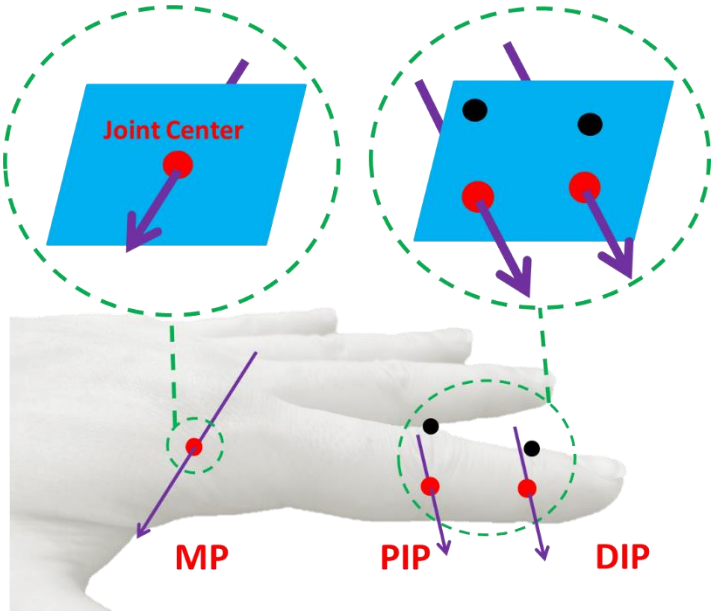

Figure 4.5 Estimation method of the joint rotation center.

4-1-4 Construction method of the skeletal finger model

As described in 2-2, the skeletal model is important for motion measurement and estimation. The skeletal finger model is generated from the motion capture data at the reference posture, and the posture data of receivers must be calibrated in advance. Figure 4.6 presents a comparison of the local coordinates of the skeletal finger model and receivers after the advanced calibration. Figure 4.6 (a) shows the local coordinates of the receivers. The yellow vectors represent the finger bones, while the black boxes represent the receivers. Figure 4.6 (b) shows the local coordinates of skeletal finger model. The yellow lines represent the finger bones. The origins of the local coordinates are at the distal side of each finger bone. For example, the origin of the distal phalanx is at the fingertip. At shown in Figure 4.6, despite the metacarpal, the orientation of the local coordinate of the finger bone is obtained after the advanced calibration described in Chapter 2. In the definition of the skeletal finger model, the local coordinate of the receiver placed on the dorsum of hand is different from the local coordinate of the metacarpal. However, the orientation of the metacarpal is not discussed in this thesis or presented in the skeletal finger model.

To generate the finger bones in the skeletal finger model, the position of the fingertip, DIP, PIP, and MP joints is necessary. Different from the orientation of the local coordinate, the origin of the finger bone is not the same as the receivers. Figure 4.7 shows calculation method of finger bones. The position of the DIP, PIP, and MP joints is at the joint rotation center, and the details of calculation are described in 4-1-2. The fingertip is the middle point of the distal edge of the nail, which is measured with the stylus. From the position of the DIP, PIP, and MP joints, the vectors that represent the finger bones can be obtained.

The last step of generating the skeletal finger model is to attach the orientation of the local coordinate to each finger bone, which can either link the data of the bone and the orientation receiver or replace the local coordinate of the finger bones in the analysis software.

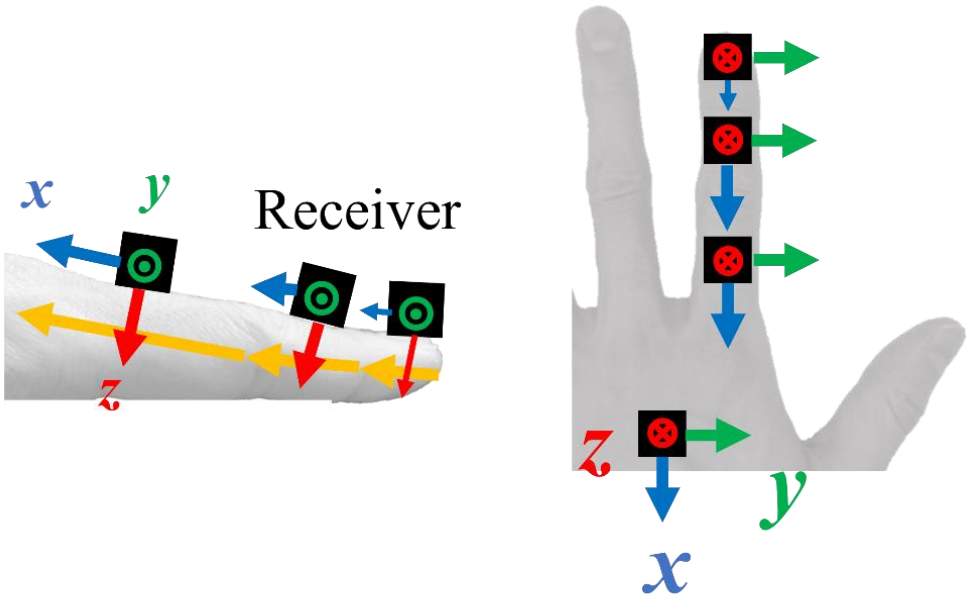

(a) Local coordinates of receivers after calibration.

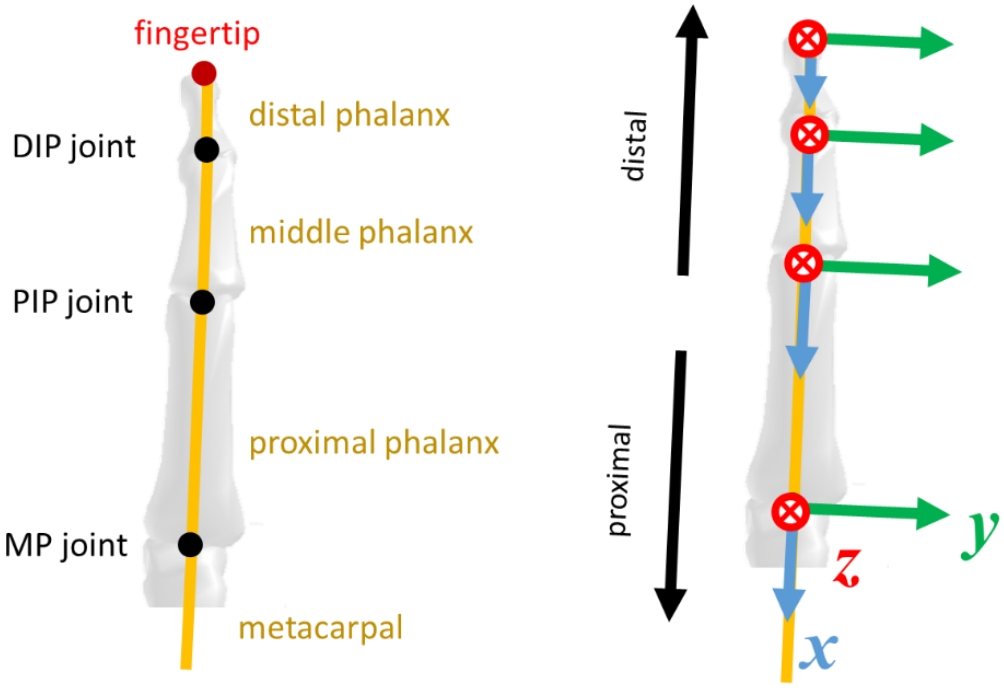

(b) Local coordinates of skeletal finger model.

Figure 4.6 Local coordinates of skeletal finger model and receivers after calibration.

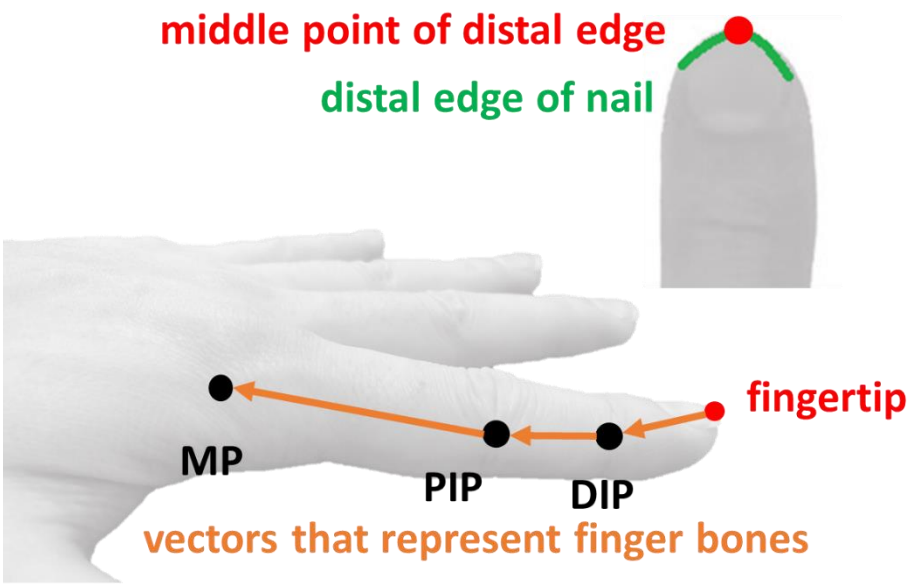

Figure 4.7 Calculation method of finger bones.

4-1-4-1 Orthogonal axis model

As shown in Figure 4.6 (b), the x axes of the local coordinate of the finger bones are in the same direction of the finger bones, while the y axes is orthogonal to the finger bones. Furthermore, the origin of the local coordinates is the same as the rotation center of the joints, and the y axes of the proximal and middle phalanx are used as the rotation axes of each joint. The Orthogonal axis model is also used by other researchers [3]-[5]. In this thesis, the skeletal finger models using the y axes as the rotation axes of joints are defined as the Orthogonal axis model. Figure 4.8 presents the Orthogonal axis model. The finger bones of the Orthogonal model also indicate local coordinates for better expression, and all local coordinates are not displayed in the figure. The green vectors represent the rotation axis of the joints, which are also on the y axis of the local coordinates.

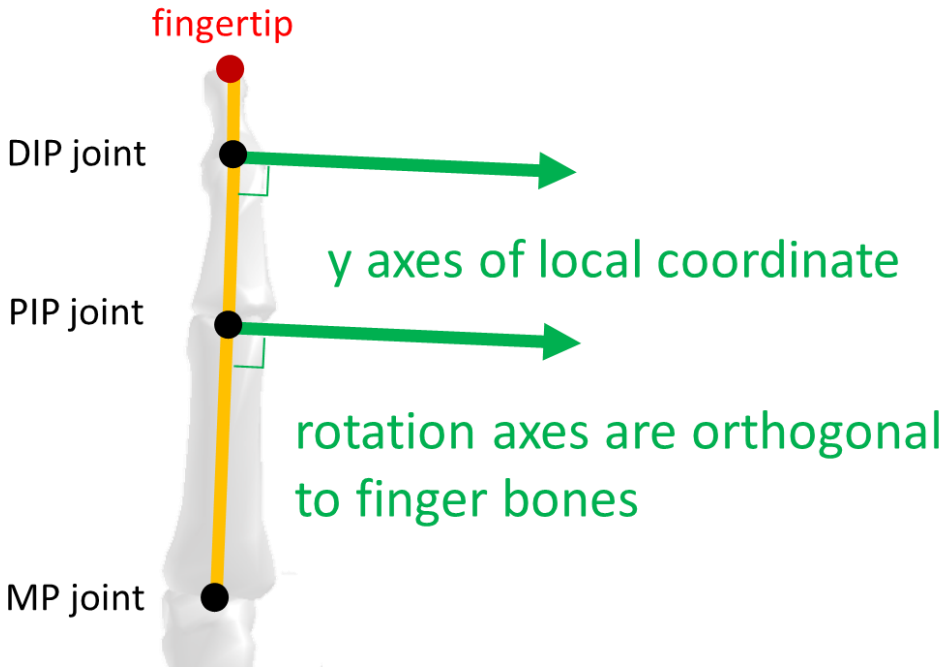

Figure 4.8 Orthogonal axis model.

4-1-4-2 User axis model

In this thesis, the User axis model is a type of skeletal finger model that is contrast to the Orthogonal axis model. In the User axis model, the axes of the finger joints are obtained with the joint axis estimation method described in 4-1-2. Because the rotation axes of each skeletal finger model are estimated from the motion data of individuals (users), the axes are usually not orthogonal to the finger bones. Figure 4.9 shows the User axis model. The purple vectors represent the rotation axis obtained with the estimation method that we proposed in this thesis. As it is shown in Figure 4.9, the rotation axes of joint fingers are not always orthogonal to finger bones.

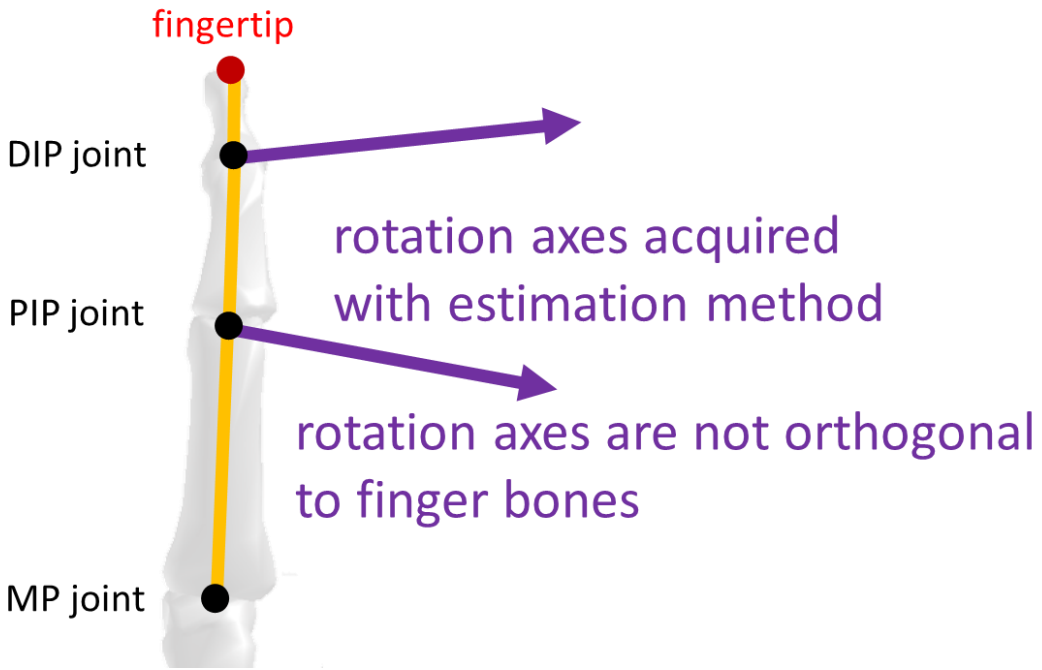

Figure 4.9 User axis model.

4-2 Evaluation of skeletal finger model

This section discusses the evaluation of the skeletal finger models generated with motion capture data we measured in our experiment. The evaluation includes the evaluation of the joint rotation axes, bone length and position of the fingertip estimated with the skeletal finger models. The details are as follows:

4-2-1 Joint rotation axes

To evaluate the axis of rotation of each joint, we calculated the distance between the axis of rotation and the rotation center in ten instances of the grasping motion. Figure 4.10 shows the distance between the axis of rotation as estimated by our method and the rotation centers of each grasping motion calculated by Modified AJPE method. Figure 4.10 (a) shows the results for the DIP and PIP joints, the red boxes represent the results for the DIP joint, and the green boxes represent results for the PIP joint. Figure 4.10 (b) shows the results for the MP joint. As it is shown in Figure 4.10, the results for the MP joint were a larger distance than for the DIP and PIP joints. For all subjects, the mean (standard deviation) distance between the axis of rotation and the rotation center of ten grasping motions for the DIP joint was 0.2 mm (0.1 mm), and the distance was 0.3 mm (0.1 mm) for the PIP joint. It is confirmed that the rotation center of each grasping motion was distributed on the axis of rotation, and the calculation for axis of rotation was correct mathematically. We applied the t test to the distance between each joint and there was no significant difference between the DIP group and PIP group ($p > 0.05$). Meanwhile, the MP group showed no significant difference between DIP and PIP. However, we provided the results without considering subject C, for which the MP group showed a significant difference for both DIP ($p < 0.01$) and PIP ($p < 0.05$).

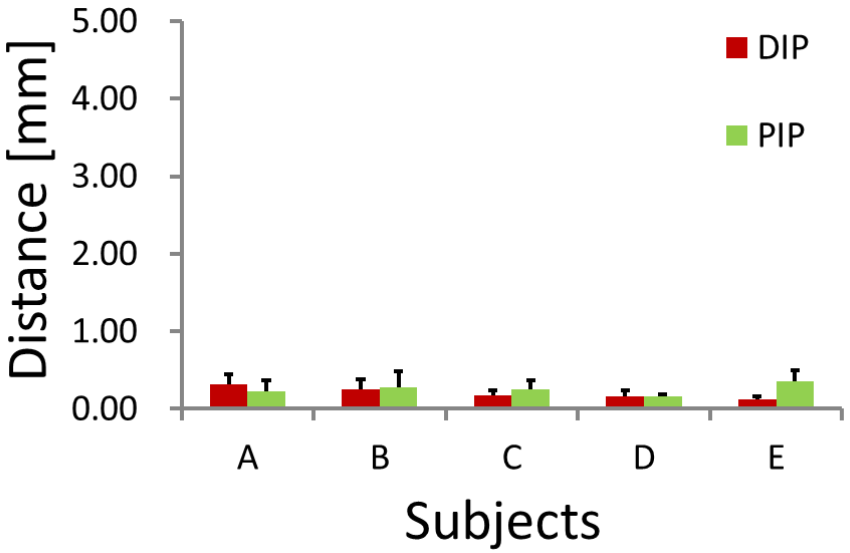

(a) DIP and PIP joints.

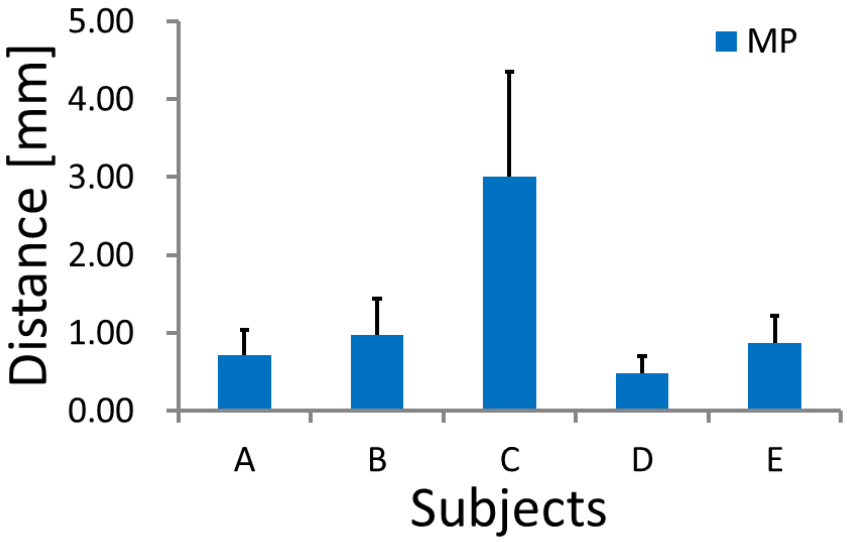

(b) MP joints.

Figure 4.10 Distance between axis of rotation estimated by our method and the rotation centers for each grasping motion.

4-2-2 Joint rotation centers

As described in 4-1-3, the vectors represent finger bones that are calculated from joint the rotation centers at reference posture. The length of the finger bones (segments) of the skeletal finger model is a constant. In order to evaluate the robustness of bone length, by utilizing 3 receivers placed on each segment of the index finger, the bone joint rotation center and variation of the finger bones length during grasping motion were analyzed. Figure 4.11 shows the motion regeneration method with 3 receivers. The positions of the joint rotation centers at reference posture can be calculated using the joint rotation center estimation method introduced in 4-1-3. Therefore, vectors represent the positional relation between the joint rotation center, and the receiver can be calculated, as represented by the blue vectors in Figure 4.11. Furthermore, with these vectors and motion data, the position of joint rotation center and the motion of finger can be estimated.

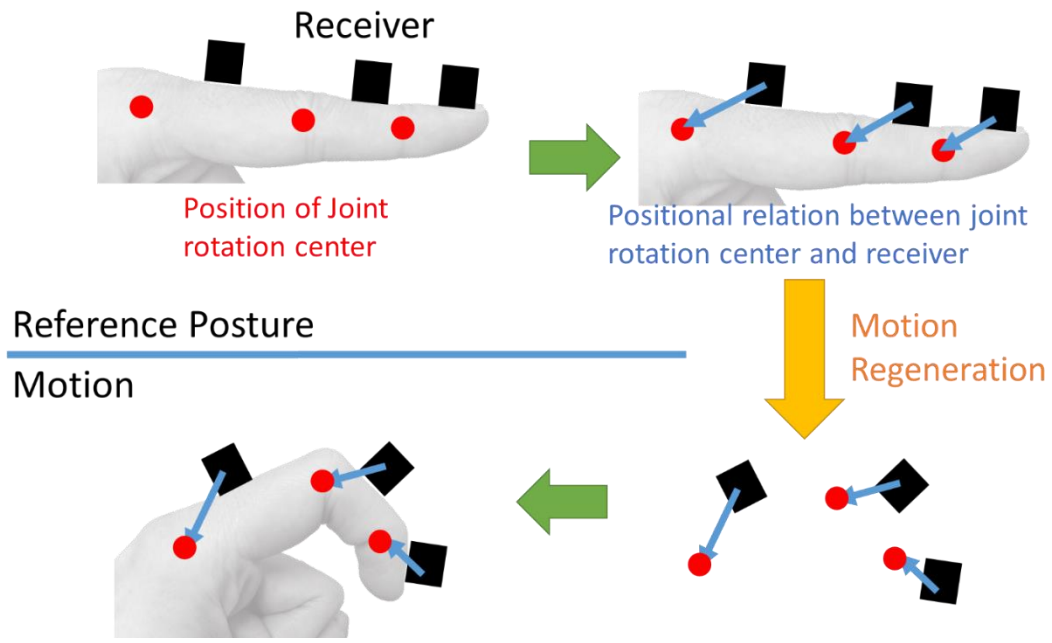

Figure 4.11 Motion regeneration method with three receivers.

Figure 4.12 shows a sample of finger segment length and joint angle during a grasping motion. The horizontal axis represents time, and the first vertical axis represents joint angle and the second vertical axis represents the length of segments. Although the angle of the PIP joint is changing (from about -20 degrees to 80 degrees) during grasping, the lengths of intermediate and proximal phalange remain stable.

Table 4.1 shows the mean and standard deviation of segment lengths for each subject (n=10). There are ten times of grasping motion measured in the experiment, and the mean finger length is defined as the length of the grasping motion. The mean and standard dedication of the ten grasping motion is calculated and shown in Table 4.1 The mean lengths of intermediate phalanges according to subjects are from 24.1 mm to 26.5 mm, and the mean lengths of proximal phalanges are from 38.3 mm to 43.3 mm. All standard deviations of estimated segment lengths are under 0.2 mm, which proved the high reproducibility of segment lengths.

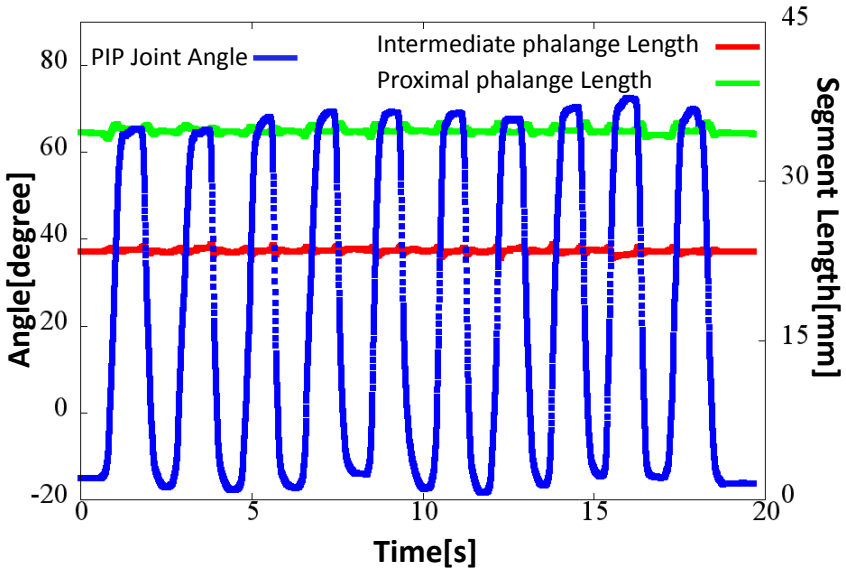

Figure 4.12 A sample of segment length and joint angle during grasping motion.

Table 4.1 Mean and standard deviation of segment lengths for each subject.

Subjects	Intermediate	Proximal
	AVE (STD) [mm]	AVE (STD) [mm]
A	24.1 (0.0)	38.3 (0.1)
B	26.2 (0.1)	43.3 (0.2)
C	25.0 (0.1)	40.2 (0.1)
D	24.5 (0.0)	40.9 (0.1)
E	26.5 (0.0)	41.5 (0.1)

Figure 4.13 shows each component of position (X, Y, Z) during ten grasping motions that were analyzed. The horizontal axis represents time and the vertical axis represents the position of center of a PIP joint. The red lines represent the components that are generated by the 2R methods, and positions generated by the 4R method are in green. The red lines are visually well polymerized to the corresponding green lines, indicating that the 2R methods are visually reliable.

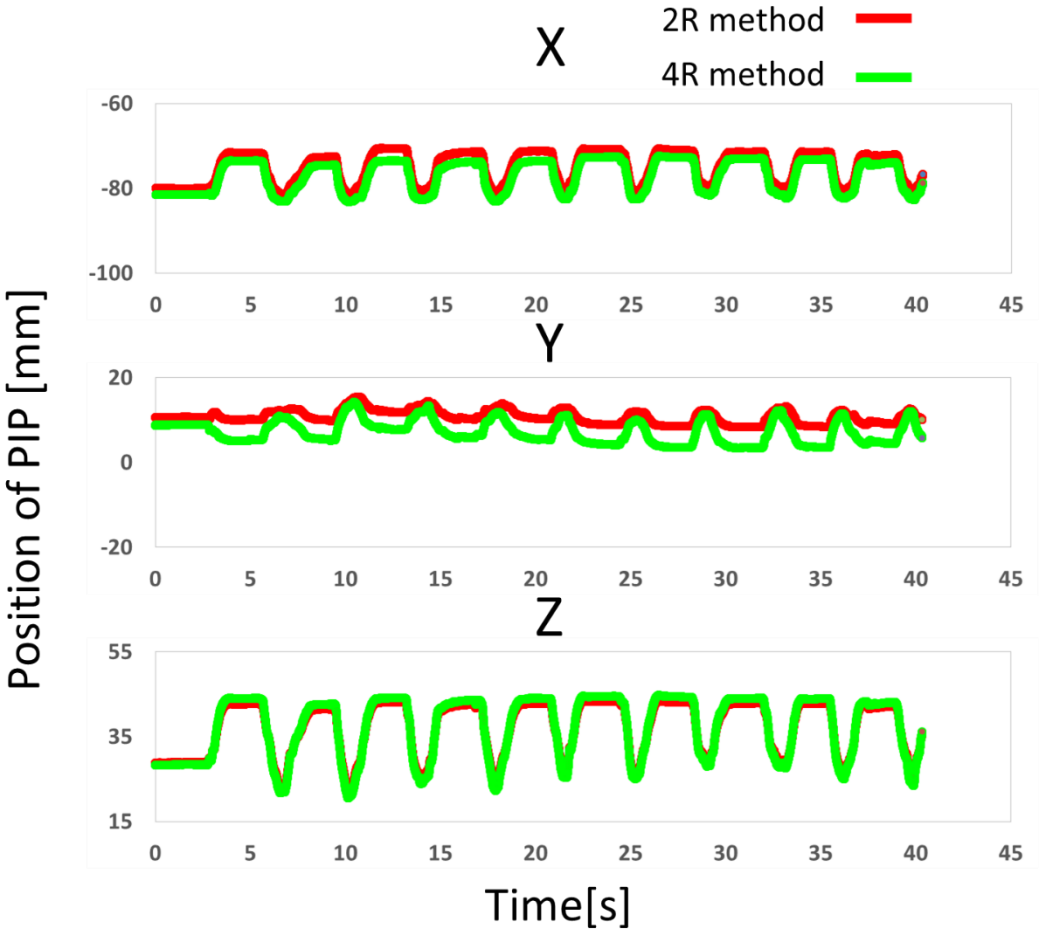

Figure 4.13 Component of position during grasping motion.

Figure 4.14 provides the validation result of the joint rotation center. The red trajectory represents the joint rotation center in the local coordinate of the bone next to the proximal side. For example, the red trajectories in the Proximal graph represent the movement of the PIP joint in the local coordinate of the Metacarpal, whose origin is at the MP joint. The blue circles represent the mean distance between the origin of the local coordinate to the trajectories. In addition, the histogram on the right side is the distribution of the distance from the red trajectories to the blue circles (error of radius). Despite the Proximal graph of subject B, the other trajectories fit well with the blue circles. With regarding to the finger joints with single rotation axes, most of the error of the radius is distributed around 0 mm. Because the origins of local coordinates are joint rotation centers, the radius blue circle also represents the mean distance between two joints (bone length). Therefore, it is proved that the joint rotation centers were estimated accurately and bone length would not change much during motion. The Y-Z plane of the Middle and Distal graph is shown as a line, which means that the PIP and DIP joints are hinge joints (single-axis joints).

On the other hand, the trajectories of the proximal phalanx are wider than others. The results confirmed that, although the grasping motion with the four fingers that are close to each other seems to be around one axis of motion for the MP joint, there is also an adduction rotation in the MP joint during the grasping. Furthermore, the trajectories in the Y-Z plane of the Middle and Distal graph are not vertical to the Y axis, which proved that the rotation axes of human fingers are different from the Orthogonal models. In addition, half of the trajectory on the Proximal graph of subject B does not coincide with the blue circle. Compared to the others, we find that the part with greater error of radius is in the range in which the Z axis is -20 mm to 0 mm. Therefore, subject B may over-extended his finger when opening his hands.

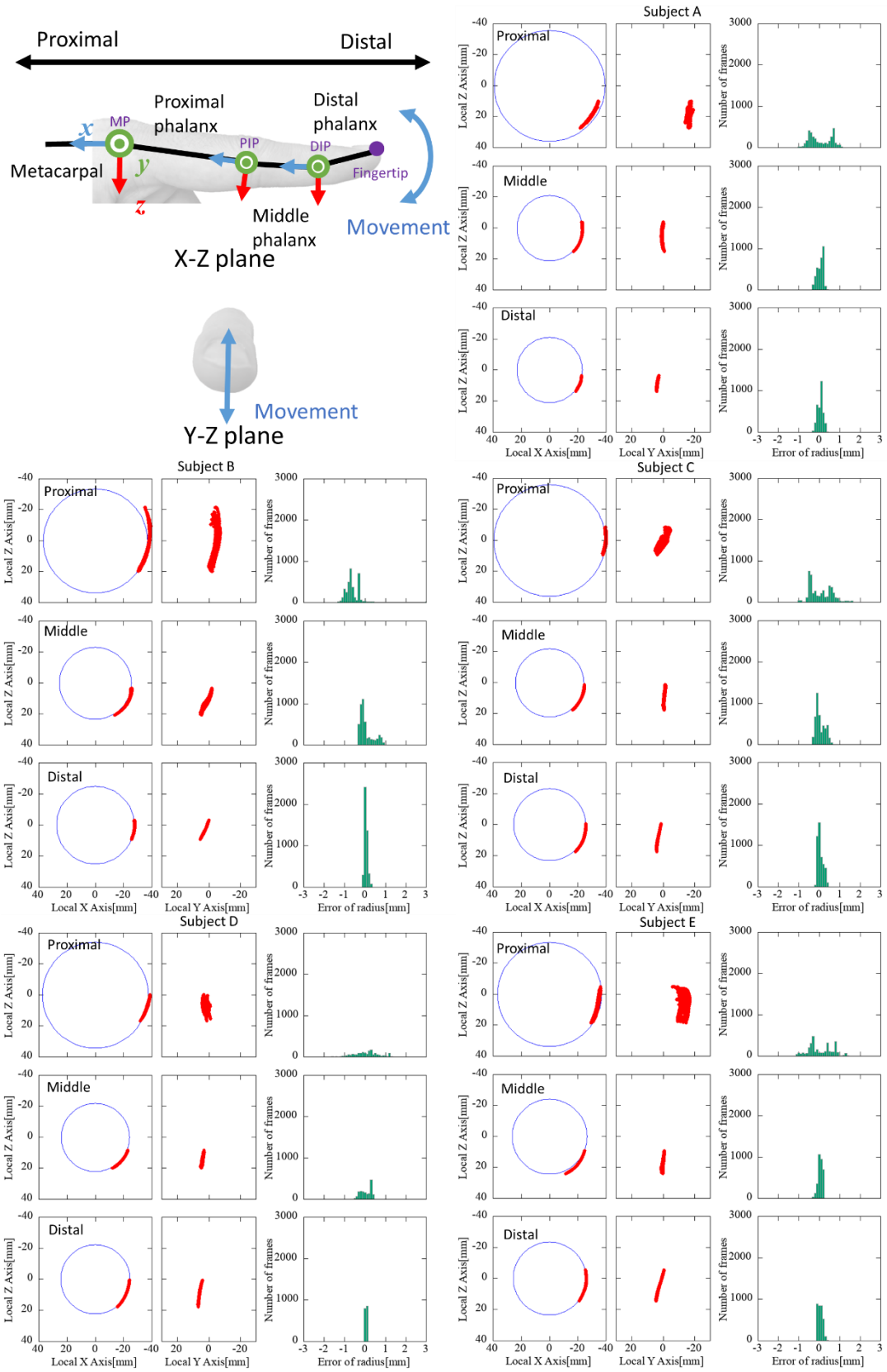

Figure 4.14 Validation result of joint rotation center.

4-2-3 Error of fingertip trajectory estimated by various methods.

Figure 4.15 shows the trajectories of the fingertips calculated with skeletal finger models and the reference position calculated from receivers placed on the distal phalanx. The green dots represent the position calculated from the motion data, and the time between each dot is 0.1 sec. Blue trajectories represent motions to the user axis model, and the red trajectories represent the orthogonal axis model. The vector of the local position of a fingertip at the coordinate of the fingertips were calculated when fingertips were measured with the stylus. With the local position vector, the fingertip positions in a grasping motion were calculated and used as the reference position. As shown in Figure 4.15 (b) and (c), the user axis model is more consistent with the reference position. In addition, Figure 4.15 (d) shows that both the user axis and orthogonal models are consistent with the reference position on a Z-X plane. This proves that errors in position increase with the finger bends. Further evaluation was done for the fingertip position when the finger was bent maximally.

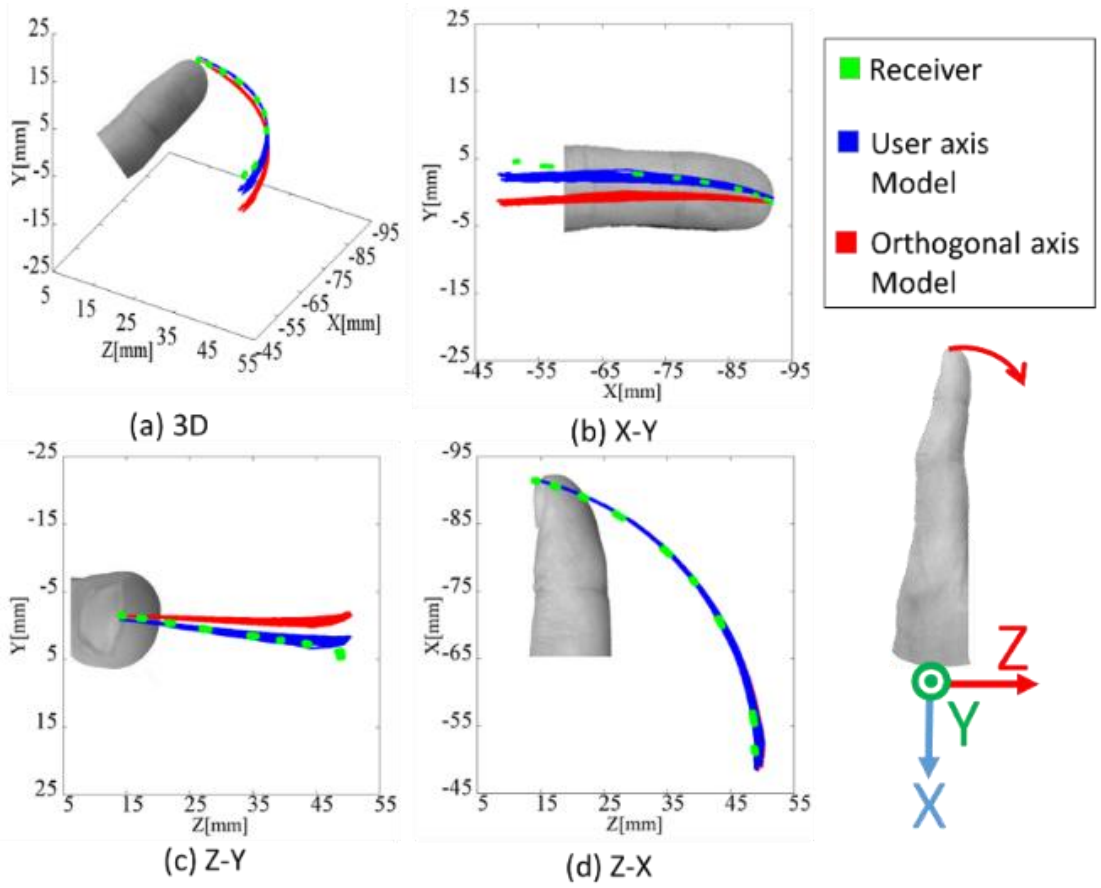

Figure 4.15 Trajectories of the fingertips calculated with skeletal finger models and the position calculated from a receiver placed on the fingertip.

Figure 4.16 shows the error in the fingertip position calculated from the user axis model and the orthogonal axis model with respect to the fingertip position calculated from the receiver placed on the fingertip when a finger was maximally bent. For each subject, we applied a t test between the user axis model and the orthogonal axis model. As a result, the error in the user axis model was significantly lower than in the orthogonal axis model ($p < 0.01$) for every subject. Compared to the error of the fingertip position calculated by the orthogonal axis model, the error of the fingertip positions calculated by the user axis model was reduced by 79% for subject B, 49% for subject D, and 63% for subject E. As it is shown in the trajectories in Y-Z planes of Middle and Distal in Figure 4.14, the Subject B,D,E are not orthogonal with Y axis, while Subject A and C are nearly orthogonal, relatively. Furthermore, when considering all subjects as one group, the mean (standard deviation) error of the fingertip positions calculated by the orthogonal axis model was 5.4 mm (3.4 mm) and was 2.7 mm (1.3 mm) in the user axis model. The t test results also show that the user axis model is significantly different from the orthogonal axis model ($p < 0.01$). Based on the above results, in the user axis model, the mean error for fingertip position was reduced by 50%, and the standard deviation was reduced by 62%. By applying a two-factor factorial ANOVA, the model factor and subject factor were interactive with each other ($p < 0.05$), and as such the results were discarded. However, there is a tendency that subject factor may have caused the differences in the results ($p < 0.05$).

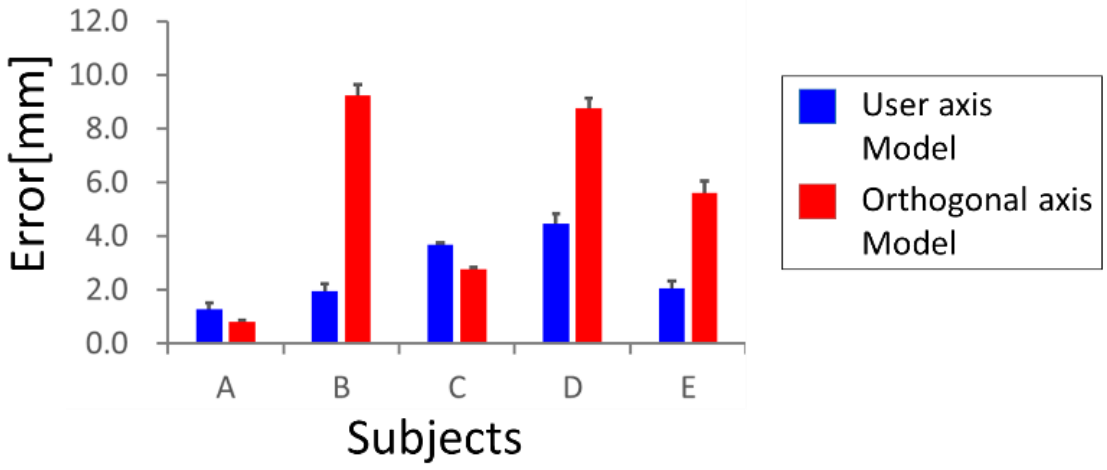

Figure 4.16 Error of the fingertip position calculated from user axis model and orthogonal axis model with respect to the fingertip reference position (n=10).

4-2-4 Error of fingertip positions estimated by various methods compared to target positions

Figure 4.17 shows the distribution of error for the fingertip position calculated with a user axis model and an orthogonal axis model and the fingertip position calculated from the receiver placed on a fingertip with respect to the target position when reaching the target. The target position was represented by a notch on the chemical wood. The triangle represents the position calculated from the receiver placed on the distal phalanx, the circle represents the fingertip position estimated by the user axis model, and square represents the fingertip position estimated by the orthogonal axis model. The color of the marks represents which target the index finger reached, which is green at 20 mm and black at 120 mm. For both skeletal finger models, the lighter the color, the smaller the distance between the fingertips of the thumb and index finger. This shows that to a target position from 20 mm to 80 mm, the error in the end points were gathered, while at over 100 mm the errors shifted towards a plus position.

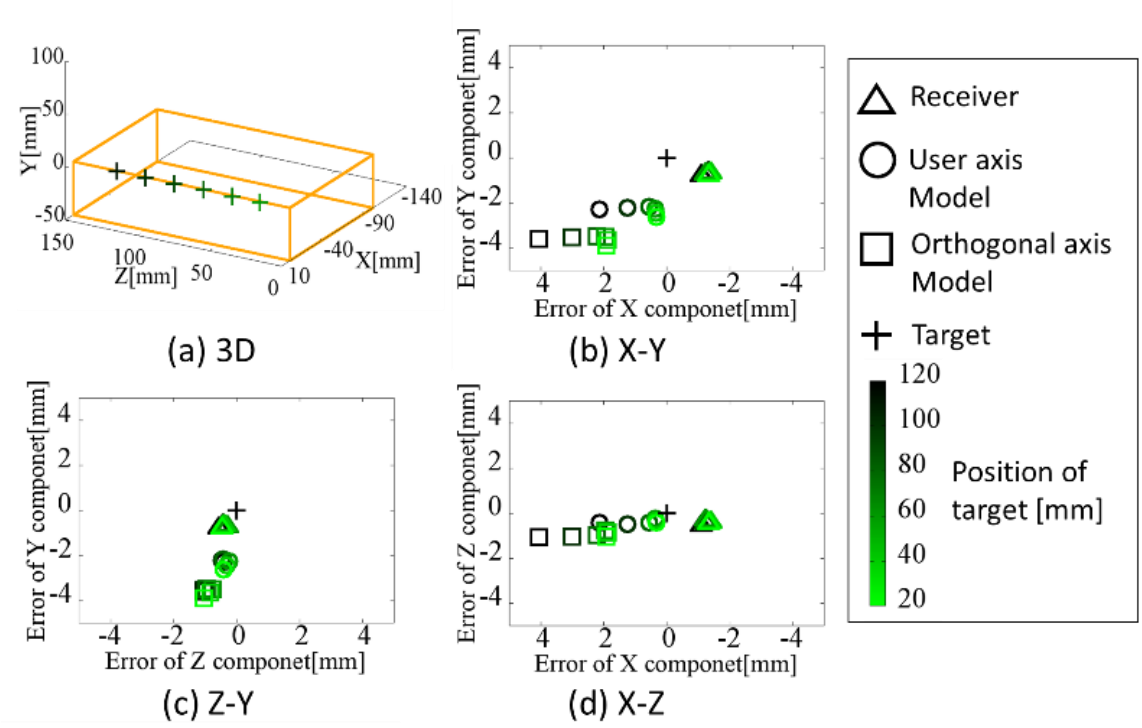

Figure 4.17 Distribution of error of fingertip position calculated with user axis model and the orthogonal axis model and the fingertip position calculated from the receiver placed on the fingertip with respect to the target position when reaching the target.

Figure 4.18 shows the mean and standard deviation of error of the fingertip position calculated with the user axis model and the orthogonal axis model and the fingertip position calculated from the receiver placed on a fingertip with respect to the target position when reaching the target (n=5). Green boxes represent the error of the fingertip positions calculated from the data of the receiver attached to the distal phalanx, the blue boxes represent the user axis model and the red boxes represent the orthogonal axis model. The mean (standard deviation) error of fingertip positions calculated with the user axis model to all target positions was 2.6 mm (0.9 mm), while the orthogonal axis model was 4.7 mm (1.7 mm). Furthermore, the two-factor factorial ANOVA shows that there was no interaction with the error and the target position ($p > 0.05$), and there was a significant difference between the user axis model and orthogonal axis model. From the discussion above, using user axis model resulted in a mean error of fingertip position that was reduced by 45%, and the standard deviation was reduced by 47% compared to the orthogonal axis model.

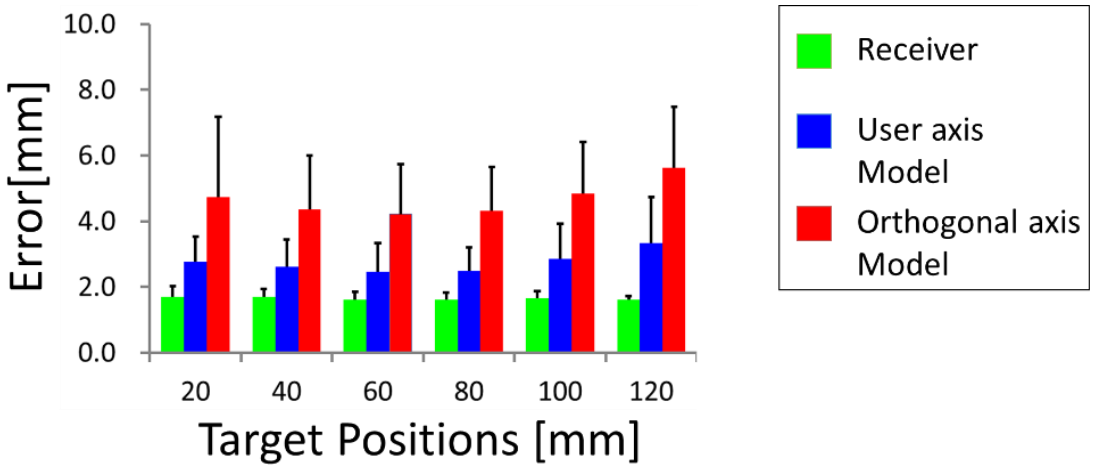

Figure 4.18 Mean and standard deviation of error of the fingertip position calculated with the user axis model and the orthogonal axis model and the fingertip position calculated from the receiver placed on a fingertip with respect to the target position when reaching the target (n=5).

4-3 Summary

This chapter introduces a construction and evaluation method for a skeletal finger model. In particular, this chapter introduces a construction method for a model that captures both orthogonal axes and a user axis model. Furthermore, evaluations are done to consider variations of finger bone length, joint rotation axes and fingertip positions of both the orthogonal model and user axis model. The results proved the robustness of the skeletal finger model construction method. Next chapter introduces an estimation method of joint center positions utilizing two receivers attached on fingertip and hand dorsum.

<References>

[1] C. M. SHAKARJI, “Least-squares fitting algorithms of the NIST algorithm testing system,” J. Res. Nat. Inst.Stand. Techn., Vol.103, Issue. 6, pp.633–641, (1998).

[2] J.F. O’Brien, R.E. Bodenheimer, G.J. Brostow, J.K. Hodgins, “ Automatic joint parameter estimation from magnetic motion capture data,” Graphics Interface Conference, pp.53-60, (2000).

[3] Y. Endo, S. Kanai, T. Kishinami, N. Miyata, M. Kouchi, M. Mochimaru, “Optimization-Based Grasp Posture Generation Method of Digital Hand for Virtual Ergonomic As sessment,” SAE International Journal of Passenger Cars - Electronic and Electrical Systems, Vol.1, No.1, pp.590-598, (2009).

[4] J. Butterfaß, M. Grebenstein, H. Liu, G. Hirzinger, “DLR-Hand II: Next generation of a dexterous robot hand,” In Proc. IEEE Int. Conf. Robotics and Automation, pp.109-114, (2001).

[5] K.S. Fok, S.M. Chou, “Development of a finger biomechanical model and its considerations,” Journal of Biomechanics, Vol.43, Issue.4, pp.701–13, (2010).

Chapter 5 Estimation and evaluation method for motion of finger segments that no receivers placed on

Previous chapters in this thesis introduced and discussed the construction method of skeletal finger models from motion data of individuals, by utilizing a magnetic motion capture system with high position and orientation resolution. However, one more problem that needs to be addressed is physical collision between instruments and magnetic receivers. When using scissor-like tools, the handler may collide with magnetic receivers. Figure 5.1 shows the area that instruments and receivers may potentially collide with each other. In order to reduce physical collision between instruments and receivers, receivers can only be placed on the fingertips and dorsum of the hand.

Therefore, this chapter introduces a method to estimation method for motion of finger segments that no receivers placed on, by utilizing the skeletal finger models constructed with method that proposed in Chapter 4.

Positions and posture finger segments without receivers can be calculated with Inverse Kinematics (IK) methods. There are several IK solutions for computing the position or posture via estimation of each segment of a link structure. Some solutions of IK problems are tasked as a problem of finding a local minimum of a set of non-linear equations [1]. One famous IK method in a biomechanically constrained situation is the Cyclic Coordinate Descent (CCD) algorithm [2], which is a heuristic iterative method with low computational cost for each joint per iteration without matrix manipulations. One IK solution that has a very low computational cost is the triangulation method [3]. Although the method has been improved, especially for unnatural looking problems for n-link IK problems, it is hard to apply to joint limits, which means that is hard to control the path in a 3D space. Because the triangulation can reach the target via one iteration, it has greater performance benefits over CCD. Our proposed method is based on the triangulation method. As our IK problem is focused on the hand, the solution to this typical problem can be improved by adding constraints and estimation methods for special conditions. One of the special conditions we want to introduce is finger over extension, which usually is discussed in motion capture [4], but has rarely been considered in inverse kinematics.

Figure 5.1 Area that instruments and receivers may potentially collide with.

5-1 Finger motion estimation method

In this finger motion estimation method proposed here, there are two kinds of conditions. Figure 5.2 shows the inverse kinematic method for estimating finger segments without receivers. Figure 5.2 (a) shows the method for flexion, which is the main movement of a grasping motion. Figure 5.2 (b) shows the method for over extension, which commonly happens when stretching the fingers, but is usually not taken into consideration. We made a condition judging vector $\boldsymbol{v}_{co}^{i}$, which is the cross product of $\boldsymbol{v}_{dt}^{i}$ and $\boldsymbol{v}_{dm}^{i}$. By comparing the $\boldsymbol{y}_i$ local coordinate of the receiver placed on the fingertip with $\boldsymbol{v}_{co}^{i}$, the finger pose condition is determined. At flexion posture, $\boldsymbol{v}_{co}^{i}$ is in the same direction of $\boldsymbol{y}_i$, and would be in a reversed direction with an over extension posture. With the corresponding calculation method, the joint center could be calculated. By importing a skeletal hand model, the position of the DIP and MP ($\boldsymbol{p}_{dip}^{i}$, $\boldsymbol{p}_{mp}^{i}$) joints can be calculated from the motion data of the receivers placed on the fingertips and dorsum of a hand. Our method is shown in pseudo-code in algorithm 5.1.

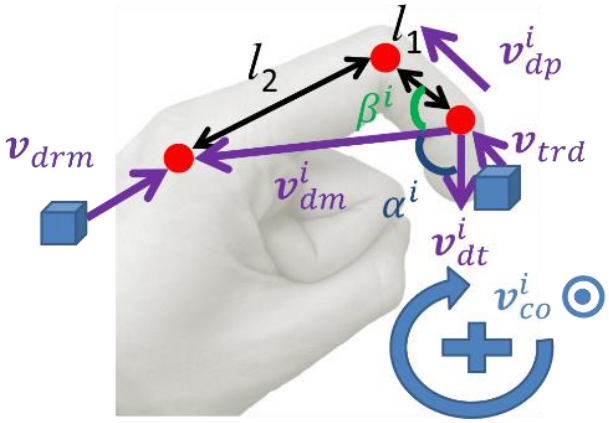

(a) Flexion.

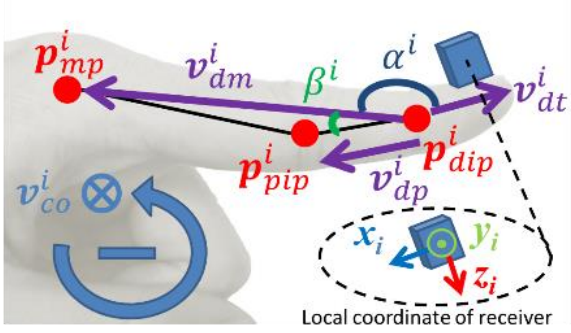

(b) Over extension.

Figure 5.2 Finger segment position estimation method for flexion and over extension posture.

Algorithm 5.1 Joint center estimation method

Input motion data (#position (*x,y,z*) and posture (*yaw, pitch, roll*) of receivers placed on fingertips and dorsum of the hand)
Input $\boldsymbol{v}_{drm}$, $\boldsymbol{v}_{trd}$, l_1, l_2 (#skeletal hand model)
for all frame *i* **do**
calculate $\boldsymbol{p}^i_{mp}$, $\boldsymbol{p}^i_{dip}$, $\boldsymbol{v}^i_{dt}$, $\boldsymbol{v}^i_{dm}$
if $|\boldsymbol{v}^i_{dm}| \geq l_1 + l_2$ **then** (#Hand at stretching posture. Sometimes, l_1, l_2 and $\boldsymbol{v}^i_{dm}$ did not form a triangle. This situation is neither flexion nor over extension.)
$\theta^i = 180°$
else
$\beta_i = \arccos(\frac{{l_1}^2+|\boldsymbol{v}^i_{dm}|+{l_2}^2}{2l_1\boldsymbol{v}^i_{dm}})$
$\boldsymbol{v}^i_{co} = \boldsymbol{v}^i_{dt} \times \boldsymbol{v}^i_{dm}$ (#Left hand coordinate)
calculate $\boldsymbol{y}_i$ (#The y-axis vector of local coordinate of receiver placed on fingertip)
if $\boldsymbol{v}^i_{co}$ and $\boldsymbol{y}_i$ are in the same direction **then**
$\theta^i = \alpha^i + \beta^i$ (#Flexion)
else
$\theta^i = -(\alpha^i + \beta^i)$ (#Over extension)
end if
end if
calculate $\boldsymbol{n}^i_{dp}$ (#Unit vector of $\boldsymbol{v}^i_{dp}$ from rotating $\boldsymbol{v}^i_{dt}$ by θ_i about $\boldsymbol{y}_i$)
calculate $\boldsymbol{v}^i_{dp}$ (#Change the length of $\boldsymbol{n}^i_{dp}$ to l_1)
calculate $\boldsymbol{p}^i_{pip}$ (#The position of PIP by translating $\boldsymbol{p}^i_{dip}$ with $\boldsymbol{v}^i_{dp}$)
end for

5-2 Evaluation method for estimated finger motion

Figure 5.4 shows the trajectories of joint centers of an index generated by the method using a full set of four receivers (4R method) and the proposed method with only two receivers (2R method) during one grasping motion that is described in a 3D space. The origin of this space is the local coordinate of the receiver placed on the dorsal side. The red trajectory represents the center of a PIP joint, and yellow represents a MP joint. Meanwhile, the green and blue trajectory represents the center of a PIP and MP joint generated by the 4R method. The trajectory of a PIP joint generated by the 2R method (red) are coincident with the trajectory generated by the 4R method (green). On the one hand, the trajectory of the MP joint generated by the 2R method are gathered as a point, while the trajectory of the MP joint generated by the 4R method are in an arc shape.

Because the MP joint estimated by the 2R method is calculated from the data of the receiver placed on dorsum of hand, which is the same as the origin of the coordinate, the MP joint estimated by the 2R method is shown as a point.

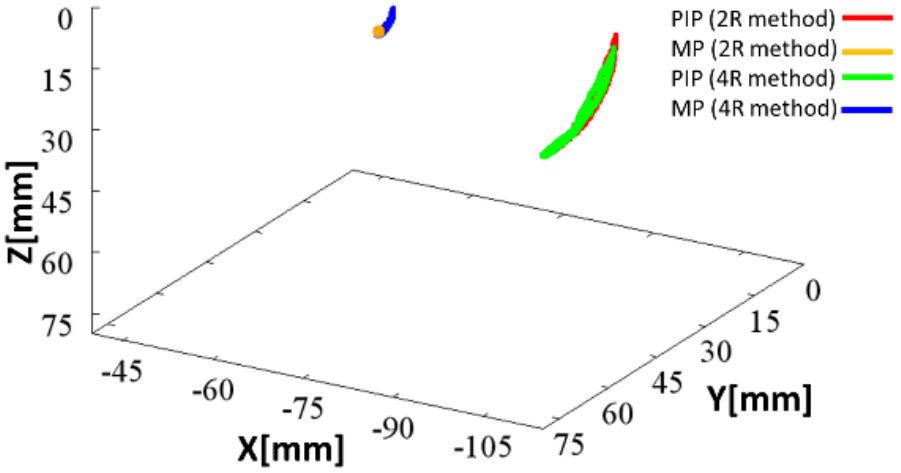

Figure 5.4 One sample of the trajectories generated by 2R method and 4R method during one grasping motion.

For a statistical evaluation, we also calculated the Pearson correlation coefficient of the lines in green and red. Table 5.1 shows the Pearson correlation coefficients between the center of the PIP joints generated by the 2R method and 4R method. For the Y component, despite subject B, correlation coefficient of others are above 0.86, which showed a strong correlation. For the X and Z components, the lowest correlation was 0.96, and both showed a very strong correlation. Table 5.2 shows the mean and standard deviation of the distance between joint centers generated by the 2R method and 4R method. The mean distance of the PIP and MP joint are under 5.6 mm, and the corresponding standard deviations are under 1.5 mm. In the inverse kinematics method, the calculation of PIP joints uses the position of a MP joint, and the standard deviation of PIP joints was greater than for MP joints in most cases. The standard deviation of MP joints are under 1.1 mm.

From table 5.1 and 5.2, we can conclude that the MP joint and PIP joint estimated by the 2R method we proposed in this thesis are consistent with the result of 4R method. However, except subject C, the Y components of subjects are relatively lower than other components. Because of the 2R method we proposed in this thesis is using orthogonal axes, the error in the rotation axes may be the cause of the error in Y component. Therefore, if develop an estimation method that considering the rotation axes of individuals, it is possible to improve the estimation accuracy of the 2R method.

Table 5.1 Pearson correlation coefficients between the center of PIP joints generated by 2R method and 4R method.

Subjects	Pearson correlation coefficients		
	X	Y	Z
A	0.98	0.95	0.98
B	0.98	0.65	0.99
C	0.96	0.99	0.98
D	0.99	0.93	0.99
E	0.99	0.86	0.99

Table 5.2 Mean distance between joint center of generated by 2R method and 4R method.

Subjects	Mean (SD) distance [mm]	
	PIP joint	MP joint
A	2.4 (0.8)	1.5 (0.6)
B	3.4 (1.1)	1.2 (1.1)
C	2.4 (1.5)	0.7 (0.8)
D	3.3 (2.1)	0.6 (0.2)
E	5.6 (1.3)	1.3 (0.8)

5-3 Summary

By constructing a skeletal finger model from magnetic motion capture data, we were able to estimate the finger segment position of the index finger with two receivers. We proposed, introduced, and validated an inverse kinematic method for estimation. In the evaluation part, which included motion capture data from five subjects, we compared the finger segment position estimated by our method with a full set of four receivers. The Pearson correlation coefficients between the center of PIP joints generated by our method with two receivers and a method using a full set of four receivers, despite the Y component of subject B, were strong (over 0.86). The error of both PIP and MP joint are under 2.1 mm, which proved the robustness of method we proposed in this thesis.

<References>

[1] Jianmin Zhao, Norman I. Badler, “Inverse kinematics positioning using nonlinear programming for highly articulated figures,”, ACM Transactions on Graphics Vol.13, No.4, pp.313-336, (1994).

[2] Chris Welman, “Inverse Kinematics and Geometric Constraints for Articulated Figure Manipulation,” Master Dissertation, Simon Fraser University, Department of Computer Science, (1993).

[3] R. Mu ller-Cajar, R. Mukundan, “Triangulation: a new algorithm for inverse kinematics,” Proceeding of the Image and Vision Computing New Zealand 2007, New Zealand, pp.181-186, (2007).

[4] P.Braido, X. Zhang, “Quantitative analysis of finger motion coordination in hand manipulative and gestic acts,” Human Movement Sci., Vol.22, pp.661-678, (2004).

Chapter 6 Conclusion

This doctoral thesis proposed a method to generate a skeletal finger model for the estimation of finger motion when using scissor-like tools. Specifics are provided below:

(1) Development of calibration method to match the orientation of receivers to the posture of a finger.

- Instead of matching the orientation of receivers to the posture of a finger acquired visually, the calibration method calculates the posture of finger bones from the position of the joint center. This approach made it possible to adequately reduce potential errors in the calibration process.

(2) Development of a hand motion measurement system for measuring hand motion and evaluating fingertip position.

- To measure the position and posture of finger bones during a grasping motion by subjects, we designed a cylinder that is placed temporarily on a test bench for practice. Furthermore, the utilization of a stylus as a position measurement device, made it possible to measure the position of the middle point of the wrinkles of the finger joints to replicate the sagittal plane of a finger.
- To evaluate the accuracy of the fingertip (end point) position that is estimated with the skeletal finger model, we designed a target with notches (target positions) that were measured with the stylus. Thus, it was possible to quantitatively evaluate an end-point position.

(3) Development of a construction method for a skeletal finger model that considers the rotation axes of each individual.

- We developed a method to estimate the rotation axes of joints from grasping motion data.
- We developed a method to estimate the rotation centers of joints from the rotation axes, sagittal plane (estimated from middle point of the wrinkles of the finger joints measured with the stylus) and the motion data at the reference posture.
- The fingertip position of the finger models constructed with our method was evaluated with five sets of grasping motion data captured from five people. Compared to a finger model with rotation axes orthogonal to the finger bone, the mean error of the finger model generated by the proposed skeletal finger model was reduced by 45%, and the standard deviation of the finger model generated by the

proposed skeletal finger model was reduced by 47%. This proves that by utilizing the skeletal finger model generated with our method, the accuracy of fingertip position is improved.

(4) We developed a finger motion estimation method that avoids collision between receivers and scissor-like tools.

- With the parameters of the skeletal finger model, we proposed a method to estimate the position of the middle phalanx and proximal phalanx (two finger bones without attached receivers) from the motion data of receivers placed on the fingertip and hand dorsum.
- With the motion data of five people, this thesis evaluated the position of the PIP joint and MP joint which represent the position of the middle phalanx and proximal phalanx. The results found that the errors for both the PIP and MP joint were under 2.1 mm. Furthermore, we also evaluated Pearson correlation coefficients between the center of the PIP joints generated by our method with two receivers and a method using a full set of four receivers. For five people, all components (x, y, z) of four people were strong (over 0.86). Thus, the results proved the robustness of our method.

6-1 Importance of this research in engineering

Motion capture has developed considerably over the past few decades. Research about hand motion measurement has also developed and been discussed. However, the measurement of hand motion when using scissor-like tools has not developed in line with such trends. Thus, this thesis, which focuses on key technologies for finger motion measurement when using scissor-like tools, proposed an approach to generate a skeletal finger model for the estimation of finger motion with two receivers attached on the fingertip and hand dorsum. The importance of this research in engineering is as follows:

(1) The calibration process of magnetic motion capture receivers is very important for matching the orientation of receivers to finger posture. The calibration method proposed in this thesis calculates the posture of finger segments from joint centers, which is more accurate than posture that is confirmed visually, especially in the vertical direction.

(2) We developed a construction method for a skeletal finger model that involves the rotation axes of each particular individual based on data from their grasping motion. This technology is a key technology for design of a master-slave robot hand that utilizes parameters from a skeletal finger model. Furthermore, by comparing the

skeletal finger model that we proposed with a skeletal finger model with axes orthogonal to the finger bones, we proved that a skeletal finger model utilizing the rotation axes of that individual has better accuracy. The results proved that it is possible to improve the operation accuracy of general robot hands, which are designed with rotation axes orthogonal to finger segments, by changing the orientation of joint axes.

6-2 Outlook and future tasks

This thesis only addressed index fingers. However, at minimum, the middle fingers and thumb are necessary to manipulate scissor-like tools, such as laparoscopic instruments. Therefore, our future research will aim at applying our method to other fingers. As the thumb has the highest degree of freedom, the estimation method of thumb motion with receivers placed on the thumb tip and hand dorsum will be the main challenge of our future research.

Acknowledgements

The research presented in this thesis has been carried out with continuous help and assistance by many people.

First, I would like to express my sincere gratitude and appreciation to my supervisor Professor Mitobe KAZUTAKA, for the continuous support of my everyday life in PhD studies, especially for his positive attitude, technical writing and patient guidance through all the research projects.

Besides my supervisor, I would also like to sincerely express my appreciation to the following Professors: Professor Yoichi KAGEYAMA, Professor Masatoshi ARIKAWA and Professor Masaru ONODA, for their helpful suggestions and advice about technology and future research.

Thereafter, I am also sincerely grateful to Professor Noboru YOSHIMURA, for support and guidance on my research and career.

After that, I am also deeply indebted to Technical staff Masachika SAITO, for data-analysis programming, advice and helping of my understanding Japanese culture.

Furthermore, I am also sincerely grateful to Senior Lecturer Katsuya FUJIWARA, for suggestions and helping in many aspects of life. In addition, I am also sincerely grateful to Assistant Professor Sawako NAKAJIMA, for suggestions and advice about technology. Additionally, I am also sincerely grateful to Professor Masafumi SUZUKI and Associate Professor Mahmudul KABIR, for their support during my PhD studies.

Last but not the least, I would like to thank my family for understanding, valuable advice, encouragements and financial support.

Thanks for all your unwavering supports and encouragements!

Rong TANG
Akita University
January 2019

Achievements

Papers (peer review)

(1) Tang, R., Mitobe, K., Saito, M. and Yoshimura, N.:
A Method of Skeletal Finger Model Generation Considering Phalange Length and Joint Rotation Axis of Individuals. International Journal of engineering sciences & research technology, Vol.7, Issue.10, pp.20-29, (2018).

(2) Tang, R., Saito, M., Mitobe, K. and Yoshimura, N.:
Method for Simplifying Magnetic Hand Motion capture: Position and Posture Estimation Method for Finger Segments of Index with Two Receivers. International Journal of engineering sciences & research technology, Vol.7, Issue.9, pp.20-27, (2018).

Conferences

(1) Tang, R., Saito, M. and Mitobe, K.:
Development of A Method for Joint Center Estimation and Simplified Hand Motion Capture Algorithm using Six Magnetic Receivers.
ASIAGRAPH 2016 International Conference Proceedings, (Toyama, Japan), pp.57-58, (2016).

(2) 唐栄，齋藤正親，鈴木雅史，柴田傑，吉村昇，水戸部一孝
簡易型磁気式手指用モーションキャプチャ装置の構築と評価
医用・生体工学研究会，MBE-15-050, 107 頁～112 頁，(2015 年).

(3) 唐栄，水戸部一孝，齋藤正親，富岡雅弘，鈴木雅史，吉村昇
簡易型磁気式手指用モーションキャプチャ装置の開発
第 18 回日本バーチャルリアリティ学会大会論文集, 482 頁～483 頁，(2013 年).